University of Windsor

Scholarship at UWindsor

Electronic Theses and Dissertations

Theses, Dissertations, and Major Papers

2009

Load Disturbance Torque Estimation for Motor Drive Systems with Application to Electric Power Steering System

Smitha Cholakkal
University of Windsor

Follow this and additional works at: https://scholar.uwindsor.ca/etd

LOAD DISTURBANCE TORQUE ESTIMATION FOR

MOTOR DRIVE SYSTEMS

WITH APPLICATION TO ELECTRIC POWER

STEERING SYSTEM

By

Smitha Cholakkal

A Thesis

Submitted to the Faculty of Graduate Studies

through Electrical and Computer Engineering

in Partial Fulfillment of the Requirements for

the Degree of Master of Applied Science at the

University of Windsor

Windsor, Ontario, Canada

2009

Load Disturbance Torque Estimation for Motor Drive Systems with Application to Electric Power
Steering System

By

Smitha Cholakkal

APPROVED BY:

_____

Dr. Nader Zamani-Kashani
Department of Mechanical, Automotive and Materials Engineering

_____

Dr. Narayan Kar
Department of Electrical and Computer Engineering

_____

Dr. Xiang Chen, Advisor
Department of Electrical and Computer Engineering

_____

Dr. Mitra Mirhassani, Chair of Defense
Department of Electrical and Computer Engineering

22 September 2009

DECLARATION OF PREVIOUS PUBLICATION

This thesis includes 3 original papers that have been previously published/submitted for publication in peer reviewed journals, as follows:

Thesis Chapter	Publication title/full citation	Publication status*
Chapter 3,4	*"Fault Tolerant Control of Electric Power Steering using Kalman Filter-Simulation Study"; 2009 EIT Conference, Windsor,*	published
Chapter 3,4	*"Fault Tolerant Control of Electric Power Steering using Robust Filter-Simulation Study"; 2009 VPPC Conference, Dearborn*	published
Chapter 3,4	*"Fault Tolerant Control of Electric Power Steering using Hinfinity Filter-Simulation Study"; 2009 IECON Conference, Portugal*	accepted

I certify that I have obtained a written permission from the copyright owner(s) to include the above published material(s) in my thesis. I certify that the above material describes work completed during my registration as graduate student at the University of Windsor.

I declare that, to the best of my knowledge, my thesis does not infringe upon anyone's copyright nor violate any proprietary rights and that any ideas, techniques, quotations, or any other material from the work of other people included in my thesis, published or otherwise, are fully acknowledged in accordance with the standard referencing practices. Furthermore, to the extent that I have included copyrighted material that surpasses the bounds of fair dealing within the meaning of the Canada Copyright Act, I certify that I have obtained a written permission from the copyright owner(s) to include such material(s) in my thesis.

I declare that this is a true copy of my thesis, including any final revisions, as approved by my thesis committee and the Graduate Studies office, and that this thesis has not been submitted for a higher degree to any other University or Institution.

ABSTRACT

Motors are widely used in industries due to its ability to provide high mechanical power in speed and torque applications. Its flexibility to control and quick response are other reasons for its widespread use. Disturbance torque acting on the motor shaft is a major factor which affects the motor performance. Considering the load disturbance torque while designing the control for the motor makes the system more robust to load changes. Most disturbance observers are designed for steady state load conditions. The observer designed here considers a general case making no assumptions about the load torque dynamics. The observer design methods to be used under different disturbance conditions are also discussed and the performances compared. The designed observer is tested in a Hardware-in-Loop (HIL) setup for different load conditions. A motor load torque estimation based Fault Tolerant Control (FTC) is then designed for an Electric Power Steering (EPS) system.

DEDICATION

My parents, brother and sister, for their continuous encouragement and loving support.

ACKNOWLEDGEMENTS

TABLE OF CONTENTS

CHAPTER

LIST OF FIGURES

LIST OF TABLES

NOMENCLATURE

α	Slip angle
β	Vehicle side slip angle
δ	Steering angle
θ_m, θ_p	Motor,pinion angular position
ψ	Yaw angle
ω	Motor speed
a_x	Longitudinal acceleration
a_y	Lateral acceleration
B_{hw}	Handwheel viscous friction constant
B_L	Load viscous friction constant
B_m	Motor viscous friction constant
C_α	Cornering stiffness
f_e	Electrical frequency
F_y	Lateral force
G	Instrumentation amplifier gain
i_a, I_a	Motor current
J_L	Load inertial constant
J_{hw}	Handwheel inertial constant
J_m	Motor inertial constant
K_f	Stiffness coefficient
K_t	Mechanical constant
K_v	Electrical constant
L_a	Motor Armature Inductance
n	Gearbox ratio
n_s	Steering gear ratio
T_{align}	Tire aligning moment
T_d	Disturbance torque
T_{driver}	Driver torque input to steering wheel
t_m	Mechanical trail
t_M	Mechanical time constant

t_p Pneumatic trail

T_{ts} Torsion bar torque

V_t Voltage applied at motor terminals

V_x Longitudinal velocity

V_y Lateral velocity

ABBREVIATIONS

BLDC   Brushless DC motor

CAN   Control Area Network

CMRR   Common Mode Rejection Ratio

EPS   Electric Power Steering

ESP   Electronic Stability Program

FTC   Fault TolerantControl

GIMC   Generalized Internal Motor Control

GPS   Global Positioning Sensor

HIL   Hardware in Loop

INS   Inertial Navigation System

PMDC   Permanent Magnet DC motor

PMSM   Permanent Magnet Synchronous Motor

PWM   Pulse Width Modulated

SBW   Steer-By-Wire

SMC   Smart Motor Controller

CHAPTER 1

INTRODUCTION

Motors are the backbone of industrial automation. Industries use electric motors in various applications due to its ability to provide high mechanical power in speed and torque applications. Its flexibility to control and quick response are other reasons for its widespread use. In the automotive sector alone, the motor is used for traction, valve control, power steering, control of windows, sun roof, engine cooling fan, and will soon be replacing the mechanical camshaft as it improves the system efficiency due to its ability to vary the timing function. A major external factor which affects the motor system performance is the disturbance torque acting on the motor shaft. When the motor is subjected to disturbance, the measured outputs of the motor reflect this external change. For example, increase in torque acting on the motor shaft causes the speed of motor to reduce, thus reducing the back-emf of the motor. This causes the current to increase reflecting the load change. Similarly decrease in load torque or assisting torque is reflected by decrease in motor current. In a current controlled system, the change in load torque is detected by the change in voltage required to maintain the constant current. By considering the load torque on the motor shaft, better controllers could be designed to make the controlled system robust to load changes. Sensors used for control purposes reflect the disturbance torque in its output. By using a motor disturbance torque observer to estimate the disturbance load torque, the sensor signals could be replaced by an estimated value. Disturbance torque observers are used in sensor-less and Fault Tolerant Control (FTC) applications.

In this thesis, the estimation of disturbance load toque acting on the motor shaft is explored with an application case study of how this torque estimate could be used for fault tolerant control of Electric Power Steering (EPS).

1.1 Disturbance Torque Estimation

The two major outputs of a motor are speed and torque. Considering the disturbance torque on the motor shaft while designing the control makes the system more robust to load changes. The load torque estimation for a DC motor is done in [1]. The disturbance torque acting on the motor shaft is assumed to be constant with respect to the dynamics of the observer. Two methods of torque estimation are discussed. In the first method the torque is considered as an unknown input and the estimation errors are calculated. The estimation error of current is known and is used to calculate the speed estimation error and thus the disturbance torque and motor speed are calculated. In the second method the disturbance torque is considered as one of the state variables and a classical observer is designed to estimate the state variables.

In [2], the disturbance torque for field oriented induction motor drives is estimated. The motor speed is estimated by the integral of the difference between the actual torque and reference torque. This difference is considered as the acceleration of the motor and the disturbance torque can be calculated from the difference. The motor model is constructed by using the stator current and rotor flux as the state variables. A speed adaptive flux observer is designed to estimate the motor speed, from which the acceleration is determined, which is then used to estimate the disturbance torque.

Nonlinear control of a Permanent Magnet Synchronous Motor (PMSM) using load torque estimation is designed in [3]. An extended nonlinear observer is used to estimate the states of the PMSM. The PMSM model is built by considering the rotor position, the currents in the stationary two axes reference frame and the disturbance load torque as the state variables. The disturbance torque is assumed to be a slowly varying load and so its dynamics is set as zero. The observer thus estimates the load torque directly. In [4] a speed control method by load torque estimation of high performance Brushless DC motor (BLDC) drives is designed. A full state observer is

designed for the BLDC by considering the speed, position and load torque as state variables assuming the load dynamics to be very slow. The position is the measured variable used by the observer.

In [5], a projection observer [6] and Kalman observer are compared and a new method merging the two observers is designed. The discrete model of the system is considered and it was found that the encoder quantization causes the speed and disturbance torques estimates to be oscillatory. So the new observer in [5] is designed by using a projection observer near the encoder pulses and if there is no output feedback for many sampling periods, the estimated position could be greater than one encoder line. The state estimate is then updated with a constant position, adjusting the Kalman gain to the standard filter one.

A sensorless co-operation between human and mobile manipulator using disturbance torque observer is designed in [7]. The reaction torque in a manipulator is estimated using a disturbance torque observer. The disturbance torque is calculated from the acceleration of the actuator and the current input. The velocity is differentiated to obtain the acceleration and a low pass filter is inserted to reduce the noise in velocity signal. The mathematical model of the mobile manipulator is estimated by the Newton-Euler method.

It is seen that most of the observer designs consider the disturbance torque dynamics to be very slow, thus assuming it to be zero. But this may not always be true. The disturbance torque observer designed in this thesis considers the general case, making no assumptions about the load torque dynamics.

1.2 Fault Tolerant Control

Fault tolerant control based on strain gauge sensor estimate using a reaction force observer is designed in [8]. The strain gauge sensor signal is estimated by multiplying an appropriate gain to the estimated reaction force and an adaptation algorithm is applied to update of this gain to improve the estimation accuracy and estimation robustness. The fault is detected by monitoring the estimation error and the controller works with the estimated signal once the fault is detected. The effect of estimation error and estimation delay on the stability of the controlled system is also considered while designing the fault-mode controller. Loop shaping design procedure is used to design the normal mode and fault mode controllers using different weighting functions to account for the estimation error and delay.

In [9], FTC for a Steer-By Wire (SBW) system using a dual motor dual microcontroller control system is designed. Each motor uses a smart motor controller (SMC) to form an inner motor torque control loop. This torque loop controls the motor torque output to track a given torque reference. The second microcontroller forms an outer loop controlling road wheel position. Thus 2 microcontrollers in Master-Slave configuration is formed. When a fault occurs, the slave takes over. If fault occurs at one local motor loop, corresponding SMC will shut down torque control loop. SBW switches to single motor operation automatically without any intervention from master or slave microcontroller.

In [10], an active FTC with disturbance compensation is discussed using a Generalized Internal Model Control (GIMC). In this design, the residual signal is constructed by taking the filtered error between estimated output and true output and processing it through detection filter. When a fault is detected, a compensation signal is fed back to the controller through a robustification controller.

In [11], a torque sensor-less control in a multi-degree of freedom manipulator using disturbance observers is discussed. Two disturbance observers are applied at each joint to realize robust motion controller and obtain a sensor-less torque controller. The robust acceleration controller is realized by the feedback of the estimated disturbance torque. The reaction torque is calculated from the estimated disturbance torque and the dynamic model of the manipulator. The feedback of the calculated reaction torque is then utilized to realize the sensor-less torque control.

In [12], FTC of an electric power steering system is designed. A classical Luenberger observer is used to estimate the disturbance torque on the motor shaft assuming the torque dynamics to be zero relative to the system dynamics. The relationship between the torques acting on the motor shaft is then used to calculate the required torsion bar torque sensor signal which could be used when a fault occurs with the sensor.

1.3 Thesis Outline

This thesis is structured as follows: in Chapter 2, the preliminary theory required for observer design and the motor model are detailed. Different methods to design the observer gain and the significance of each method, based on its performance are provided.

In Chapter 3, the methodology to design the load torque disturbance observer for a DC motor is detailed which includes the method of developing the motor model to be used to design the observer depending on the external factors considered to act on the system.

In Chapter 4, the method used to design a fault tolerant control of an electric power steering system using a motor disturbance torque observer is detailed. The EPS model and methods used to estimate the torques acting on the system are also provided.

In Chapter 5, the Hardware in Loop (HIL) setup configuration and tests done to obtain the model of the system is detailed. The HIL results for motor load torque estimation and its application in EPS are presented and analyzed.

Finally, Chapter 6 summarizes the results, observations and makes recommendations for future work in this area.

CHAPTER 2

PRELIMINARY THEORY

2.1 Luenberger Filter[1]

The classical Luenberger observer is the simplest observer design which considers only the system model in its design and assumes no disturbance to act on the system. The estimates using a Luenberger filter are highly model dependent. Luenberger observer design by pole placement method [13] is discussed here. The purpose of the observer is to ensure that the estimation error reaches zero quicker than the system response.

Estimation error $e(t) = x(t) - \hat{x}(t), e(t) \longrightarrow 0$, when t→∞

The error dynamics are given by

$$\begin{aligned}
\dot{e} = \dot{x} - \dot{\hat{x}} &= (Ax + Bu) - (A\hat{x} + Bu) - L(y - \hat{y}) \\
&= A(x - \hat{x}) - L(C_2 x - C_2 \hat{x}) = (A - LC_2)e
\end{aligned}$$

(2-1)

The stability of error dynamics is determined by eigen-values of the observer matrix. The coefficients of the observer characteristic polynomial are then placed at the desired observer poles so as to achieve steady state estimation as quickly as possible.

Characteristic polynomial, *det(sI-(A-LC))=(s-p₁)(s-p₂)...(s-pₙ),*

where p_1, $p_2...p_n$ are the desired observer poles for steady and quick error dynamics.

As the Luenberger filter is designed for an ideal system, not taking into account any disturbance, its performance in a real world system is usually not satisfactory.

---

[1] The terms filter and observer are used alternatively to refer to the same thing, i.e., the state estimator

2.2 Kalman Filter

When the system is subjected to white noise, Kalman filter is used to estimate the state variables. Kalman filter is a recursive filter which estimates the states of a dynamic system from noisy measurements by minimizing the variance of the estimation error.

A system subjected to white noise is shown in *Figure 2.1*.
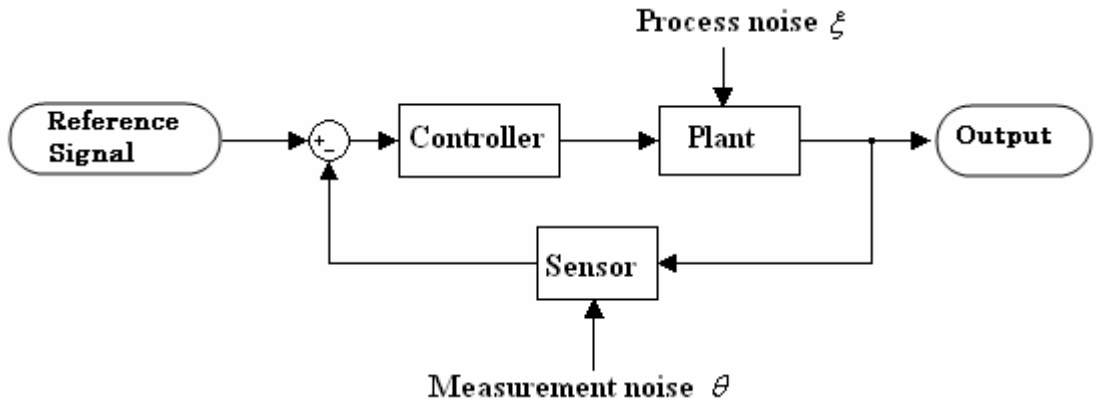
Figure 2.1. System subjected to white Gaussian noise

The state model for the system shown in *Figure 2.1* is

$$x = Ax + Bu + \xi \tag{2-2}$$

$$z = C_1 x \tag{2-3}$$

$$y = C_2 x + \theta \tag{2-4}$$

It is assumed that the average values of both the noises, ξ and θ, are zero and there is no correlation between them. Power spectral densities of the noises are Q_0 and P_0 respectively.

$$E\{\xi\} = E\{\theta\} = 0 \longrightarrow zero \ \ mean$$

$$spectrum : E\{\xi(t)\xi^T(T)\} = Q_0\delta(t-T); Q_0 = B_0B_0^T$$
$$E\{\theta(t)\theta^T(T)\} = P_0\delta(t-T); P_0 = D_{20}D_{20}^T$$

In order to represent both process noise and measurement noise by a single vector, a new noise, w_0 is introduced such that

$$\xi = B_0w_0, \ \theta = D_{20}w_0, \tag{2-5}$$

$$E\{w_0\}=0, \ E\{w_0(t)w_0(\tau)^T\}=I\delta(t\text{-}\tau). \tag{2-6}$$

The objective of Kalman filter is to minimize the cost functional, J_k, i.e., $\min\limits_{k} J_k$,

where $J_k = E\left[\int_0^\infty e^T(t)e(t)dt\right]$, e = estimation error.

This is done by solving the Riccati *equation 2-7* [14, 16, and 28].

$$(A - B_0D_{20}^T R_0^{-1}C_2)P + P(A - B_0D_{20}^T R_0^{-1}C_2)^T - PC_2^T R_0^{-1}C_2P + B_0(I - D_{20}^T R_0^{-1}D_{20})B_0^T = 0$$

$$\tag{2-7}$$

Filter gain, $L= - (B_0D_{20}^T+PC_2)R_0^{-1}$ \hfill (2-8)

Here $R_0=D_{20}D_{20}^T$.

2.3 H$_\infty$ Filter

Considering the case where the model parameters are uncertain and bound to change with time or processes, a filter which takes into account these uncertainties while estimating the state variables is required. For such a model, H$_\infty$ filter needs to be designed to make the state estimation robust to changes in model parameters. A model subjected to parameter uncertainties is shown in *Figure 2.2*.
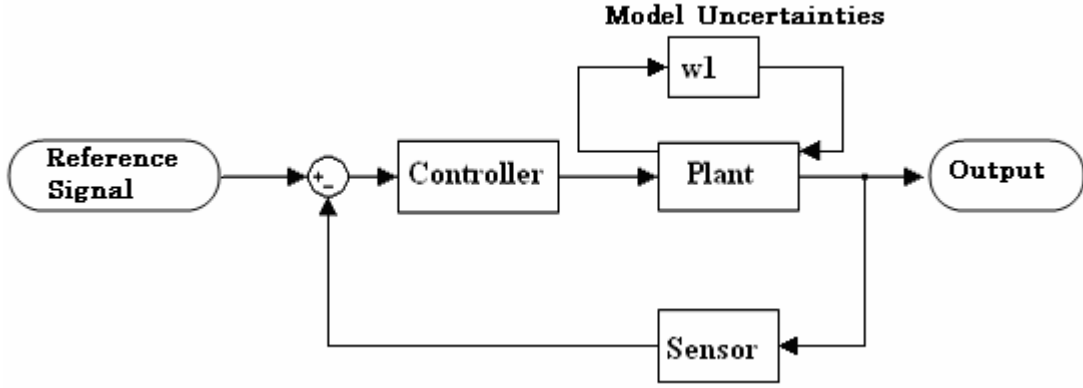
Figure 2.2. System subjected to parameter uncertainty

The system is described by the following state space model

$$\dot{x} = Ax + B_1 w; \quad x(0) = 0 \tag{2-9}$$

$$z = C_1 x + D_{11} w(t) \tag{2-10}$$

$$y = C_2 x + D_{21} w(t) \tag{2-11}$$

B_1, D_{11} and D_{21} are the weights given to the uncertainty disturbance, $w(t)$, depending on its effect on the system performance.

The H$_\infty$ filter problem is stated as:

Given a $\gamma > 0$, find a causal filter $F(s) \in RH_\infty$ if it exists such that

$$J := \sup_{w \in L_2[0, \infty)} \frac{\|z - \hat{z}\|_2^2}{\|w\|_2^2} \quad \text{with } \hat{z} = F(s) y.$$

The H$_\infty$ filter problem is considered as a special H$_\infty$ problem with no internal stability requirement compared to H$_\infty$ control. Using Theorem 14.8 [15], suppose (C_2, A) is detectable and $\begin{bmatrix} A - j\omega I & B_1 \\ C_2 & D_{21} \end{bmatrix}$ has full row rank for all ω. Let D_{21} be

normalized and D_{11} partitioned conformably as $\begin{bmatrix} D_{11} \\ D_{21} \end{bmatrix} = \begin{bmatrix} D_{111} & D_{112} \\ 0 & I \end{bmatrix}$.

Then there exists a causal F(s) $\in$ RH$_\infty$ such that $J < \gamma^2$ if and only if $\bar{\sigma} = (D_{111}) < \gamma$ and $J_\infty \in$ dom(Ric) with $Y_\infty = $ Ric(J_∞)≥ 0 where

$$\tilde{R} := \begin{bmatrix} D_{11} \\ D_{21} \end{bmatrix} \begin{bmatrix} D_{11} \\ D_{21} \end{bmatrix}^* - \begin{bmatrix} \gamma^2 I & 0 \\ 0 & 0 \end{bmatrix}$$

$$J_\infty := \begin{bmatrix} A^* & 0 \\ -B_1 B_1^* & -A \end{bmatrix} - \begin{bmatrix} C_1^* & C_2^* \\ -B_1 D_{11}^* & -B_1 D_{21}^* \end{bmatrix} \tilde{R}^{-1} \begin{bmatrix} D_{21} B_1^* & C_1 \\ D_{11} B_1^* & C_2 \end{bmatrix}$$

Y_∞ is the stabilizing solution to

$$Y_\infty A^* + AY_\infty + Y_\infty (\gamma^{-2} C_1^* C_1 - C_2^* C_2) Y_\infty + B_1 B_1^* = 0 \tag{2-12}$$

Then a rational causal filter F(s) satisfying $J < \gamma^2$ is given by

$$\hat{z} = F(s) y = \begin{bmatrix} A + L_{2\infty} C_2 + L_{1\infty} D_{112} C_2 & -L_{2\infty} - L_{1\infty} D_{112} \\ C_1 - D_{112} C_2 & D_{112} \end{bmatrix} y, \tag{2-13}$$

where $\begin{bmatrix} L_{1\infty} & L_{2\infty} \end{bmatrix} := - \begin{bmatrix} B_1 D_{11}^* + Y_\infty C_1^* & B_1 D_{21}^* + Y_\infty C_2^* \end{bmatrix} \tilde{R}^{-1}$ \hfill (2-14)

When $D_{11} = 0$ and $B_1 D_{21}^* = 0$

$$\hat{z} = \begin{bmatrix} A - Y_\infty C_2^* C_2 & Y_\infty C_2^* \\ C_1 & 0 \end{bmatrix} y \tag{2-15}$$

Here γ is the design parameter which decides the limit of uncertainty which could be tolerated by the filter for good performance. Lower the value of γ, higher the tolerance of the filter towards to model uncertainty.

2.4 H∞ Gaussian Filter

In the practical case, a system is subjected to both, white noise and parameter uncertainty. It is known that the H∞ and Kalman filter performances conflict each other. The Kalman filter is designed to achieve good performance against Gaussian noise and is model dependent, sensitive to parameter variations. The H∞ filter is designed to handle parameter uncertainty considering worst case scenario and does not give good performance with stochastic white noise. The performance of one can be improved only by sacrificing that of the other. In order to achieve a good estimate when the system is subjected to both types of disturbances, an H∞ Gaussian filter is designed based on constrained optimization result and H∞ optimization design. This filter design uses a parameter, γ which decides the weight that is given to the performance of each type of filter and thus obtains a suitable balance between the two performances.

The H∞ Gaussian filter, *F(s)* is formulated by considering the system shown in *Figure 2.3*.
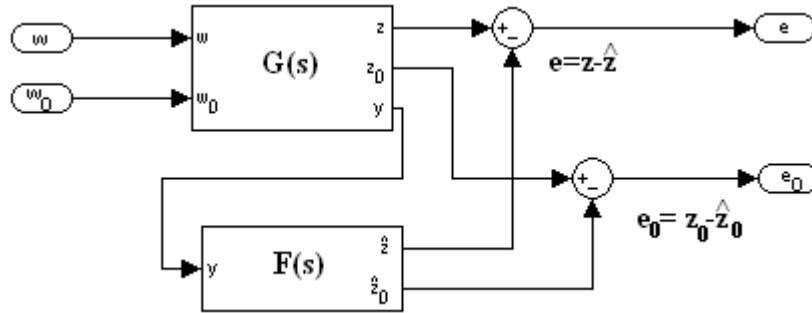
Figure 2.3. System subjected to both white noise and parameter uncertainty

The system, G(s) defined by the state equations:

$$\dot{x} = Ax + B_0 w_0 + B_1 w; x(0) = 0 \tag{2-16}$$

$$z_0 = C_0 x \tag{2-17}$$

$$z = C_1 x \tag{2-18}$$

$$y = C_2 x + D_{20} w_0; R_0 = D_{20} D_{20}^T \tag{2-19}$$

where $x(t) \in R^n$, $y(t) \in R^p$, $z(t) \in R^{q1}$, $w(t) \in R^{r1}$ (bounded power stationary signal-uncertainty), $w_0(t) \in R^{r2}$ (white noise signal), $E\{ w_0(t) \} = 0$, $E\{ w_0(t), w_0^T(\tau) \} = I\delta(t\text{-}\tau)$.

The filter $F(s)$ is in the following given form

$$\dot{\hat{x}}(t) = A\hat{x}(t) + L(C_2\hat{x}(t) - y(t)) = (A + LC_2)\hat{x}(t) - Ly(t); \hat{x}(0) = 0 \tag{2-20}$$

$$\hat{z}(t) = C_1\hat{x}(t) \tag{2-21}$$

$$\hat{z}_0(t) = C_0\hat{x}(t) \tag{2-22}$$

L is the filter gain such that estimates $\hat{z}(t)$ and $\hat{z}_0(t)$ is made as close as possible to $z(t)$ and $z_0(t)$, i.e, minimize $e(t)$ and $e_0(t)$.

For optimization purpose, the following cost functionals are defined, given a $\gamma > 0$.

$$J_1(F, w(t), w_0(t)) = \lim_{T \longrightarrow \infty} \frac{1}{T} \int_0^T E\left\{\left(\gamma^2 \|w(t)\|^2 - \|e(t)\|^2\right)\right\}dt \tag{2-23}$$

$$J_2(F, w(t), w_0(t)) = \lim_{T \longrightarrow \infty} \frac{1}{T} \int_0^T E\left\{\|e_0(t)\|^2\right\}dt \tag{2-24}$$

F is expected to be stable. Therefore we call that F is an admissible filter if its transfer function $F(s) \in RH\infty$. To formulate the H$_\infty$ Gaussian filter design problem, we need to find an admissible filter F_* in the given form of *equations 2-20 to 2-22* and a worst disturbance signal $w_*(t)$ such that $J_1(F_*, w_*(t), w_0(t)) \leq J_1(F_*, w(t), w_0(t))$ for H$_\infty$ performance and $J_2(F_*, w_*(t), w_0(t)) \leq J_2(F, w_*(t), w_0(t))$ for H$_2$ optimality hold for all F and all $w(t) \in P$.

By using Theorem 4.1 [16], for the given target system G and the cost functional J_1 and J_2, let (C_2, A) be detectable. If there are stabilizing solutions $P_1 \geq 0$ and $P_2 \geq 0$ for

$$(A - P_2 C_2^T R_0^{-1} C_2 - B_0 D_{20}^T R_0^{-1} C_2)^T P_1 + P_1 (A - P_2 C_2^T R_0^{-1} C_2 - B_0 D_{20}^T R_0^{-1} C_2) + \gamma^{-2} P_1 B_1 B_1^T P_1$$
$$+ C_1^T C_1 = 0$$

$$(2\text{-}25)$$

$$(A - B_0 D_{20}^T R_0^{-1} C_2 + \gamma^{-2} B_1 B_1^T P_1) P_2 + P_2 (A - B_0 D_{20}^T R_0^{-1} C_2 + \gamma^{-2} B_1 B_1^T P_1)^T - P_2 C_2^T R_0^{-1} C_2 P_2$$
$$+ B_0 (I - D_{20}^T R_0^{-1} D_{20}) B_0^T = 0,$$

$$(2\text{-}26)$$

where $R_0 = D_{20} D_{20}^T$. The filter gain is obtained by solving these 2 coupled Riccati *equations 2-21 and 2-22* for P_1 and P_2 and the gain is

$$L_* = -(P_2 C_2^T + B_0 D_{20}^T) R_0^{-1}$$

$$(2\text{-}27)$$

The filter F^* is

$$\dot{\hat{x}}(t) = (A - P_2 C_2^T R_0^{-1} C_2 - B_0 D_{20}^T R_0^{-1} C_2) \hat{x}(t) + (P_2 C_2^T + B_0 D_{20}^T) R_0^{-1} y(t); \hat{x}(0) = 0,$$

$$(2\text{-}28)$$

$$\hat{z}(t) = C_1 \hat{x}(t),$$

$$(2\text{-}29)$$

$$\hat{z}_0(t) = C_0 \hat{x}(t),$$

$$(2\text{-}30)$$

and the worst disturbance signal $w_*(t) = \gamma^{-2} B_1^T P_1 e_x(t) = \gamma^{-2} B_1^T P_1 (x(t) - \hat{x}(t))$ under white noise achieves

$$J_1(F_*, w_*(t), w_0(t)) \le J_1(F_*, w(t), w_0(t))$$

$$(2\text{-}31)$$

$$J_2(F_*, w_*(t), w_0(t)) \le J_2(F, w_*(t), w_0(t)).$$

$$(2\text{-}32)$$

The design parameter, γ, is chosen so as to fulfill the performance requirements of the system towards white noise and uncertainty disturbances. As $\gamma \rightarrow \infty$, the performance of filter towards white noise improves, approaching H_2 filter. Lower the value of γ, better the filter performance towards model uncertainty.

2.5 DC Motor Model

A Permanent Magnet DC (PMDC) motor is considered here. The DC motor may be represented electrically by a resistance in series with an inductance. When the rotor rotates, due to the electromagnetic induction, a back emf is generated which is proportional to the speed of the rotor. Motor being an electromechanical system has electrical and mechanical laws governing its function.
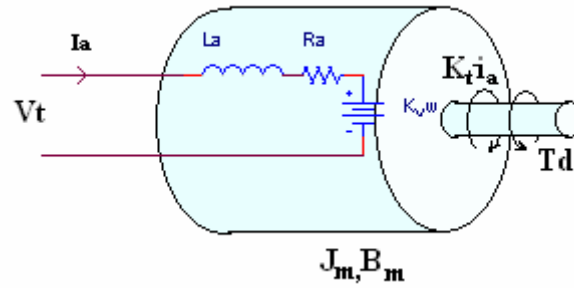
Figure 2.4. DC motor system

From *Figure 2.4*, applying Kirchhoffs voltage law,

$$V_t = i_a R_a + L_a \frac{di_a}{dt} + K_v \omega \tag{2-33}$$

The generated torque is proportional to the current flowing through the armature as the field excitation is fixed in a PMDC.

Balancing the torques acting in the system

$$K_t i_a = J_m \frac{d\omega}{dt} + B_m \omega + T_d \tag{2-34}$$

Thus the general state model for a PMDC motor is

$$x = Ax + Bu , \tag{2-35}$$

$$y = C_2 x , \tag{2-36}$$

where

$$x = \begin{bmatrix} i_a \\ \omega \end{bmatrix}; u = V_t$$

$$A = \begin{bmatrix} -\dfrac{R_a}{L_a} & -\dfrac{K_v}{L_a} \\ \dfrac{K_t}{J_m} & -\dfrac{B_m}{J_m} \end{bmatrix}; B = \begin{bmatrix} \dfrac{1}{L_a} \\ 0 \end{bmatrix}; C_2 = \begin{bmatrix} 1 & 0 \end{bmatrix}$$

Since the load disturbance torque is an external unpredictable factor and cannot be modeled, it is considered as an uncertainty disturbance and is not included in the general state model.

CHAPTER 3

LOAD DISTURBANCE TORQUE ESTIMATION FOR MOTOR DRIVE SYSTEM

The observer for the motor model is designed by considering the state space model of the system.

3.1 Constructing State Space Model to Design Observer

When constructing the state space model of the system to design the observer, some factors must be considered.

- *The state model should be observable*

  Condition for observability should be satisfied, i.e, rank of observability matrix, *O*, should be equal to number of states, *n*.

  $O = [C\ CA\ CA^2\ ....\ CA^{n-1}]^T;\quad rank(O) = n$ for an observable system

- *The variables to be estimated and their relation with the state variables.* Care should be taken to see that there is no redundancy while selecting the state variables. For example in the DC motor case, the disturbance torque acting on the motor shaft has the relation with current and speed as shown in *equation 2-30*. When there is no other specific equation which defines its dynamics with respect to the other 2 variables; T_d cannot be selected as a state variable without having redundant equations.

- *The disturbances acting on the system*

  The effect of the disturbance on the system is considered while designing the state space model and is expressed by assigning higher weights to those disturbances which affect the system more than the others.

■ *Open loop estimation or closed loop estimation.*

In open loop estimation, the controller dynamics is not considered when designing the observer. When a closed loop estimator is designed, the controller transfer function is also considered as part of the system whose state variables are estimated. The system state model is built including the controller parameters [17]. Open loop estimation can be used in any situation while closed loop estimation may be better in cases of smart motors where the motor controller and motor is available as a single unit.

3.2 Observer Design

As the required variable to be estimated in this case is the disturbance torque acting on the motor shaft, a law which relates it with the state variables is used.

$$T_d = K_t i_a - J_m \frac{d\omega}{dt} - B_m \omega \qquad (3\text{-}1)$$

In this case the load dynamics, J_L and B_L are also included in the estimation of T_d. When it is required that the T_d estimate includes only the external load disturbance torque, *equation 3-1* is changed to

$$T_d = K_t i_a - (J_m + J_L) \frac{d\omega}{dt} - (B_m + B_L) \omega \qquad (3\text{-}2)$$

where J_L, B_L = equivalent load inertial and viscous friction constants on the motor shaft.

The observer model is a replica of the system model with faster dynamics. *Table 3.I* shows the state space model of a general system and its observer.

Table 3.I State space model of a general system and its observer

General System model(excluding external disturbances)	Observer model
$\dot{x} = Ax + Bu$ $z = C_1 x$ $y = C_2 x$	$\dot{\hat{x}} = A\hat{x} + L(\hat{y} - y) + Bu$ $\hat{z} = C_1 \hat{x}$ $\hat{y} = C_2 \hat{x}$

Here x = state variables, u = inputs, z = desired outputs, y = measured outputs, L = filter gain.

The observer model used for the DC motor is shown in *Figure 3.1*.
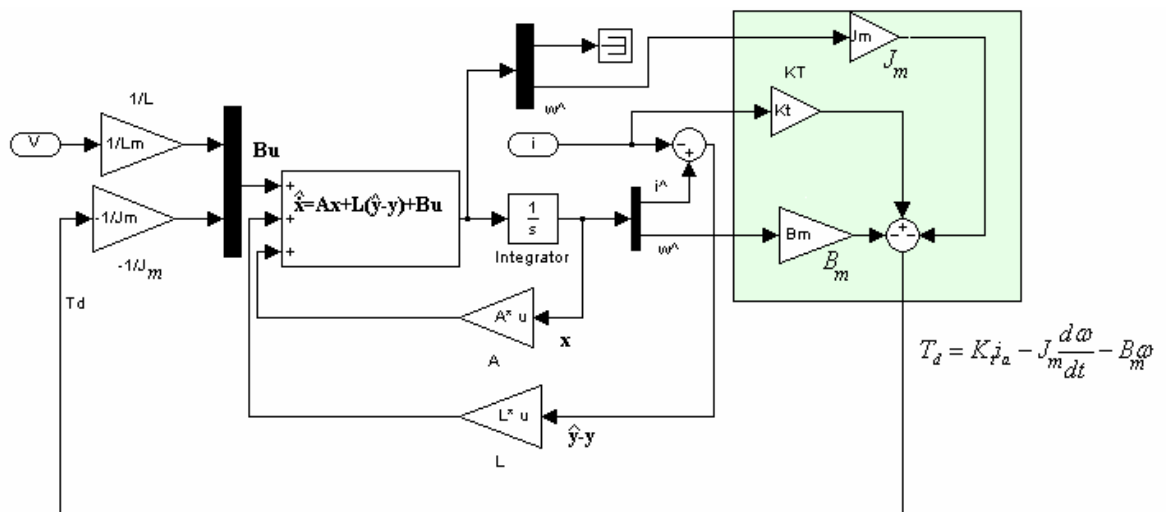
Figure 3.1. DC motor observer design

Here the disturbance torque is considered as an external disturbance, which is estimated and fed back to update the model dynamics. This feedback loop is important as it updates the system states considering the last obtained disturbance torque estimate. Without this loop, the model does not consider the effect of disturbance torque on the state variables. The filter gain L may be designed by using different methods depending on the types of disturbances affecting the system.

3.3 Luenberger Filter

The Luenberger filter is designed based on the motor model alone, and does not consider any unmodeled disturbance or external factors. The model used to design the Luenberger filter is the general motor model given by *equations 2-35* and *2-36*.

As a rule of thumb, the poles of the observer are usually chosen to converge 10 times faster than the poles of the system. However that results in very high observer gains which lead to peaking phenomenon where the initial estimation error is too high leading to instability. So the poles of the characteristic equation are selected such that the error dynamics is quicker than the fastest dynamics in the system, which in this case is the current dynamics. The current dynamics is measured and the electrical frequency, f_e (reciprocal of electrical time constant) determined. The filter gain L is designed by placing the poles of the characteristic equation greater than a factor of at least 2-3 times f_e.

3.4 Kalman Filter

In the DC motor, white noise originates from the commutator, when the brushes make and break contact with the commutator, vibration, Pulse Width Modulated (PWM) control signals, measurement noises etc.

The motor model used to design the Kalman filter in form of *equations 2-35* and *2-36* is given as

$$
\begin{bmatrix} \dot{i}_a \\ \dot{\omega} \end{bmatrix} = \begin{bmatrix} -\dfrac{R_a}{L_a} & -\dfrac{K_v}{L_a} \\ \dfrac{K_t}{J_m} & \dfrac{B_m}{J_m} \end{bmatrix} \begin{bmatrix} i_a \\ \omega \end{bmatrix} + \begin{bmatrix} -\dfrac{1}{L_a} \\ 0 \end{bmatrix} V_t + B_0 w_0
\tag{3-3}
$$

$$z = \begin{bmatrix} 1 & 0 \\ 0 & 1 \end{bmatrix} \begin{bmatrix} i_a \\ \omega \end{bmatrix} \tag{3-4}$$

$$y = \begin{bmatrix} 1 & 0 \end{bmatrix} \begin{bmatrix} i_a \\ \omega \end{bmatrix} + D_{20} w_0 \tag{3-5}$$

The weight D_{20} is set by measuring the covariance of measurement noise, P_0. The process noise covariance is relatively difficult to measure. The motor is subjected to unmodeled disturbances; hence the sensor output is more reliable than the process model. Thus Q_0 is chosen to be larger than P_0 and tuned by trial and error methods. The Kalman filter gain is then computed using *equations 2-7* and *2-8*.

3.5 H$_\infty$ Filter

It is seen that resistance is one of the major parameter uncertainties in a DC motor. Friction between brushes and commutator leads to wear of brushes and the effective resistance is found to increase with time. Also when the motor is energized, increase in temperature due to I^2R loss causes the resistance to change.

The motor model used to design H$_\infty$ filter is

$$\begin{bmatrix} \dot{i}_a \\ \dot{\omega} \end{bmatrix} = \begin{bmatrix} -\dfrac{R_a}{L_a} & -\dfrac{K_v}{L_a} \\ \dfrac{K_t}{J_m} & \dfrac{B_m}{J_m} \end{bmatrix} \begin{bmatrix} i_a \\ \omega \end{bmatrix} + \begin{bmatrix} -\dfrac{1}{L_a} \\ 0 \end{bmatrix} V_t + \begin{bmatrix} -\dfrac{1}{L_a} w_1 & 0 \\ 0 & -\dfrac{1}{J_m} w_2 \end{bmatrix} w \tag{3-6}$$

$$z = \begin{bmatrix} 1 & 0 \\ 0 & 1 \end{bmatrix} \begin{bmatrix} i_a \\ \omega \end{bmatrix} + D_{11} w \tag{3-7}$$

$$y = \begin{bmatrix} 1 & 0 \end{bmatrix} \begin{bmatrix} i_a \\ \omega \end{bmatrix} + D_{21} w \tag{3-8}$$

The disturbance vector, w is taken as $w = \begin{bmatrix} i_a \Delta R_a \\ T_d \end{bmatrix}$. T_d is considered as one of the uncertainties. D_{11} and D_{21} are considered to be zero. The weights w_1 and w_2 are chosen depending on the significance of the particular uncertainty on the model performance. The filter gain is then calculated using *equations 2-12* to *2-15*.

3.6 H$_\infty$ Gaussian Filter

The motor model for designing the H$_\infty$ Gaussian filter is built by combining the models used for Kalman and H$_\infty$ filter.

$$\begin{bmatrix} \dot{i_a} \\ \dot{\omega} \end{bmatrix} = \begin{bmatrix} -\dfrac{R_a}{L_a} & -\dfrac{K_v}{L_a} \\ \dfrac{K_t}{J_m} & \dfrac{B_m}{J_m} \end{bmatrix} \begin{bmatrix} i_a \\ \omega \end{bmatrix} + \begin{bmatrix} -\dfrac{1}{L_a} \\ 0 \end{bmatrix} V_t + B_0 w_0 + \begin{bmatrix} -\dfrac{1}{L_a} w_1 & 0 \\ 0 & -\dfrac{1}{J_m} w_2 \end{bmatrix} w \qquad (3\text{-}9)$$

$$z = \begin{bmatrix} 1 & 0 \\ 0 & 1 \end{bmatrix} \begin{bmatrix} i_a \\ \omega \end{bmatrix} \qquad (3\text{-}10)$$

$$y = \begin{bmatrix} 1 & 0 \end{bmatrix} \begin{bmatrix} i_a \\ \omega \end{bmatrix} + D_{20} w_0 \qquad (3\text{-}11)$$

The above model is used to compute the H$_\infty$ Gaussian filter gain using *equations 2-25* to *2-27*. When the inertia of the system is very low indicating very fast system dynamics, it is seen that a higher value of γ is required for stable solutions to *equations 2-25* and *2-26*. This shows that observers designed for low inertia systems show better performance towards white noise and lesser tolerance towards model uncertainty.

CHAPTER 4

CASE STUDY – FAULT TOLERANT CONTROL OF ELECTRIC POWER STEERING

The application of motor disturbance torque estimation in fault tolerant control of electric power steering (EPS) is explored in this chapter.

4.1 Electric Power Steering System

The working of EPS can be explained by using *Figure 4.1*.
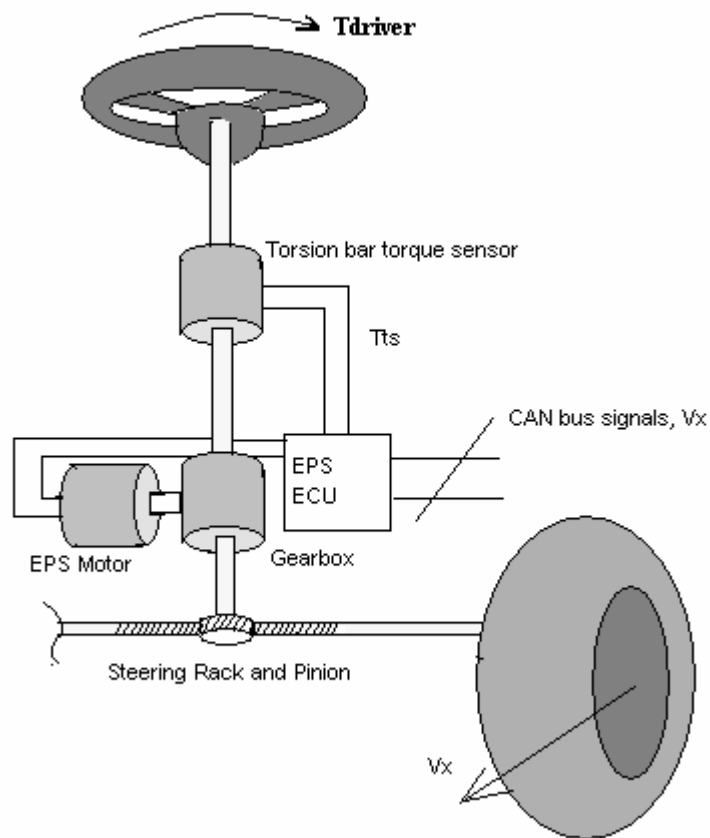
Figure 4.1. Electric power steering model

The driver applies a torque, T_{driver} to the steering wheel. This torque is transmitted to the steering rack and pinion through the torsion bar. The torsion bar deformation is sensed and the driver input torque is measured by the torsion bar torque sensor, which sends an equivalent voltage signal, T_{ts}, to the EPS controller. The EPS controller uses the signal T_{ts} and the vehicle speed signal to determine the amount of assist to be provided by the motor, then sends an appropriate signal to the motor controller. The EPS motor is thus controlled to provide more assist at low speeds and less assist at high speeds to provide better road feel to the driver. The EPS motor provides the necessary torque through the gearbox to the steering rack and pinion which steers the vehicle wheels accordingly. When a fault occurs with the torsion bar torque sensor, the EPS controller assumes no driver torque signal is sent and does not power the assist motor. This turns the EPS system to manual steering requiring the driver to provide the entire steering torque. This is an undesirable situation. To make the EPS system more reliable, a fault tolerant control using motor load torque observer is designed.

4.2 Electric Power Steering Model

The EPS model is shown in *Figure 4.2*.
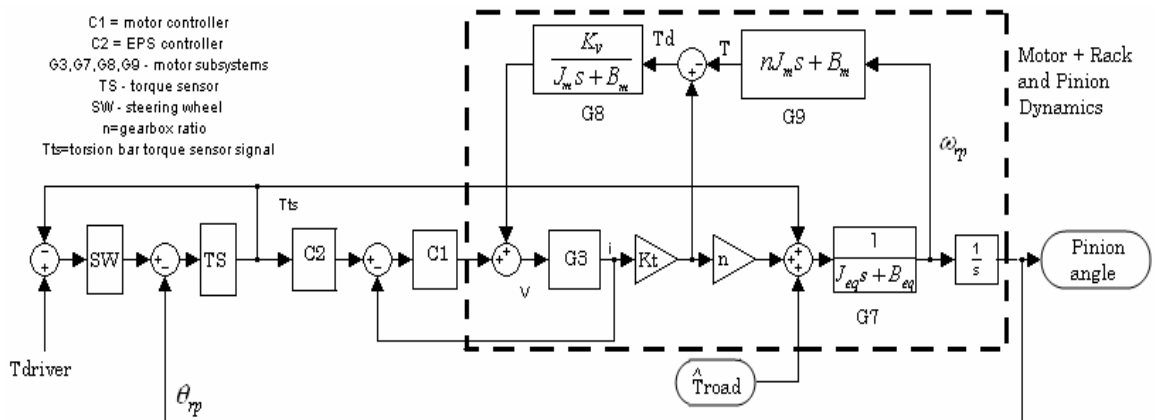
Figure 4.2. Electric power steering model in Simulink

The blocks in *Figure 4.2* can be explained as follows. T_{driver} is the torque exerted by driver to control the vehicle direction. T_{ts} is the torsion bar torque.

Steering Wheel Dynamics (SW)

The steering wheel inertia and viscous friction mainly affect the dynamics of the steering wheel angle for a steering torque applied by the driver.

$$G_{sw}(s) = \frac{\theta_{hw}}{T_{driver} - T_{ts}} = \frac{1}{J_{hw}s^2 + B_{hw}s + K_{hw}} \tag{4-1}$$

J_{hw}, B_{hw} and K_{hw} are the inertial, viscous friction and stiffness constants for the hand-wheel; θ_{hw} is the hand-wheel angle.

Torsion bar Dynamics (TS)

The difference between the torques at the two ends of the torsion bar causes a small deformation of the torsion bar. This deformation is measured and converted to a voltage signal representing the mechanical torque by the torsion bar torque sensor.

$$G_{ts}(s) = \frac{T_{ts}}{\theta_{ts}} = B_{ts}s + K_{ts} \tag{4-2}$$

$$\theta_{ts} = \theta_{hw} - \theta_p \tag{4-3}$$

B_{ts} and K_{ts} are the viscous friction and stiffness constants of the torsion bar, θ_{ts} is the deformation angle, θ_p is the pinion angle. The torsion bar torque, T_{ts} acts on the motor shaft and driver steering wheel. The electrical signal of the torsion bar sensor is sent to the EPS controller, C2, which may be designed as a simple proportional controller

or H$_\infty$ controller if model uncertainty is considered [29].

Motor Controller (C1)

Motor controller is a simple PI controller which uses the output of the EPS controller as the reference current for required torque.

$$G_c = \frac{K_p s + K_i}{s} \tag{4-4}$$

Motor Subsystems

G3, G7, G8 and G9 are motor subsystems [18, 19] as explained here.

Motor Dynamics (G3)

$$G_3(s) = \frac{i_a}{v} = \frac{J_m s + B_m}{(J_m s + B_m)(L_a s + R_a + R_f) + K_e K_t} \tag{4-5}$$

Equivalent rack and pinion dynamics (G7)

$$G_7(s) = \frac{\omega_p}{T} = \frac{1}{(J_{rp} + n^2 J_m)s + (B_{rp} + n^2 B_m)} \tag{4-6}$$

Here *T* is the total torque acting on the rack and pinion.

$$T = K_t i_a + T_{ts} + T_{road} \tag{4-7}$$

Torque/Voltage Conversion (G8)

$$G_8(s) = \frac{v_d}{T_d} = \frac{K_v}{J_m s + B_m} \tag{4-8}$$

Here v_d is the disturbance voltage due to the disturbance torque, T_d.

Speed/Torque Conversion (G9)

$$G_9(s) = \frac{T}{\omega_{rp}} = n(J_m s + B_m)$$

Having obtained the model of the system, the fault tolerant control is designed.

4.3 Fault Tolerant Control Design

It is seen that the torsion bar torque is available in two forms – electrical and mechanical. While the electrical signal is sent to the EPS controller, the mechanical signal acts on the EPS motor shaft and also counterbalances the torque on the hand-wheel. When a fault occurs with the sensor, only the electrical signal is lost while the mechanical torque continues to act. Thus by estimating the disturbance torque acting on the motor shaft, the torsion bar torque signal can be reconstructed. The fault tolerant control design is shown in Figure 4.3.
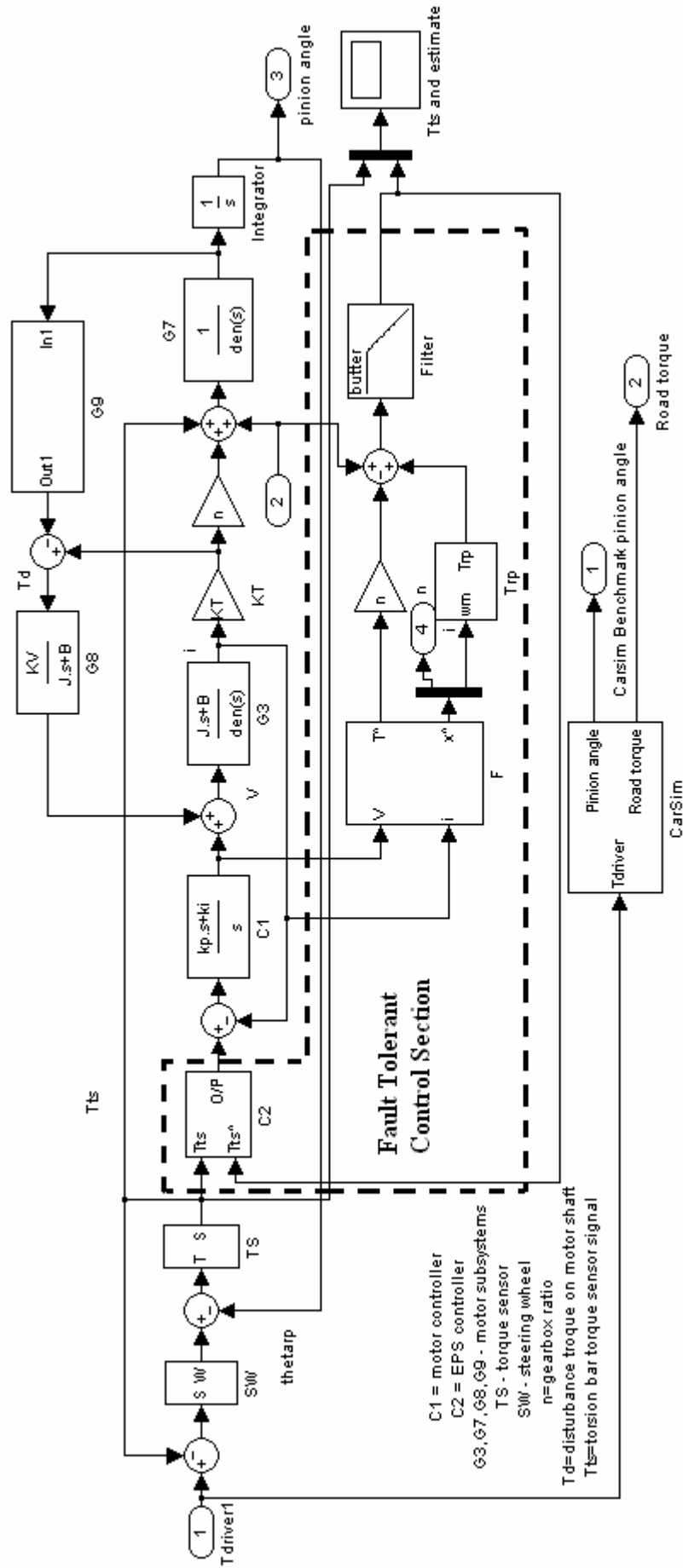
Figure 4.3. Fault Tolerant Control model of EPS in Simulink

The following equation shows the relation between the torques acting on the motor shaft

$$nT_m + T_{road} + T_{ts} = J_{rp}\dot{\omega}_p + B_{rp}\omega_p$$

(4-10)

From the *equation 4-10*, it is understood that the load or disturbance torque acting on the motor shaft is composed of road reaction torque, T_{road}, torsion bar torque, T_{ts} and the rack and pinion reaction torque, T_{rp}.

With this knowledge, the equation that relates the disturbance torque on the motor shaft, T_d, to the steering torque command, T_{ts} is formed.

$$T_d = \frac{-T_{ts} + T_{road} + T_{rp}}{n}$$

(4-11)

Thus by estimating T_d and T_{road}, T_{ts} can be reconstructed. T_{rp} can be calculated separately using the equation

$$T_{rp} = J_{rp}\dot{\omega}_p + B_{rp}\omega_p ; \omega_p = \frac{\hat{\omega}_m}{n}$$

(4-12)

The pinion speed and acceleration is obtained from the motor speed and acceleration estimates from the observer.

By rearranging equation 4-11, the torsion bar torque, T_{ts} is estimated by using *equation 4-13*.

$$T_{ts} = -(nT_d - T_{road} - T_{rp})$$ (4-13)

The fault in the torsion bar torque sensor is detected by calculating the residual, R_{ts}

$$R_{ts} = \left| T_{ts} - \hat{T}_{ts} \right|$$ (4-14)

Here T_{ts} is the measured torsion bar torque signal from the sensor and $\hat{T}_{ts}$ is the estimated value obtained from *equation 4-13*. When the fault residual, R_{ts} is greater than a threshold value, K, that indicates a fault occurrence and the estimated value, $\hat{T}_{ts}$ is used by the controller in place of the measured value. The threshold value, K is determined from experiments to ensure that the FTC is done only for hard fault such as the complete failure of the torque sensor and not for slow drifting faults.

EPS Controller (C2)

The fault tolerant control (C2) structure is shown in *Figure 4.4*.
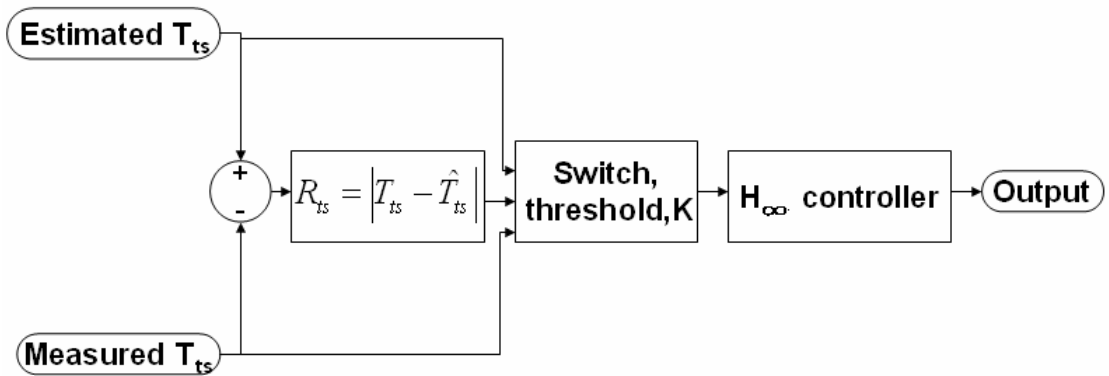
Figure 4.4. Fault tolerant controller structure

The fault residual is computed and the measured value gets replaced by the estimated value when the residual exceeds the threshold value. An H_∞ controller is used to account for the system uncertainties. The controller is designed by first considering the plant alone excluding the motor and its controller. To design the H_∞ controller, the entire plant and controller is divided into 2 sections as shown in *Figure 4.5*.
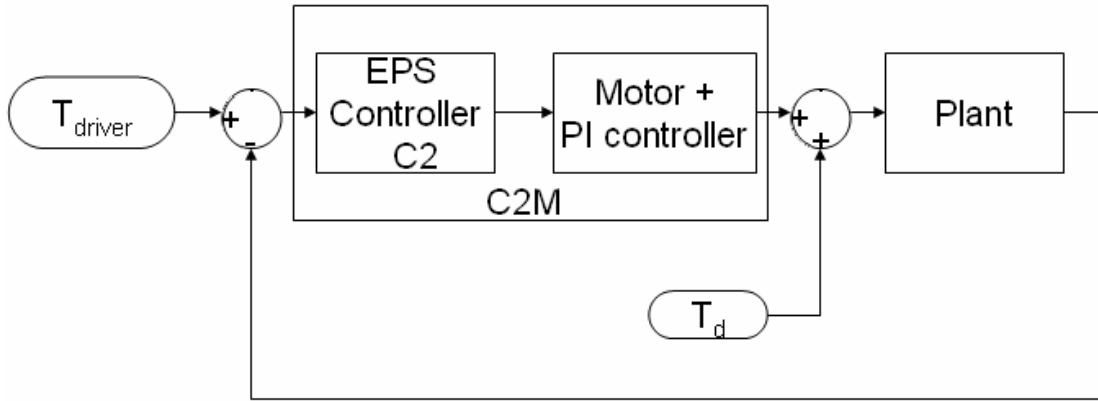
Figure 4.5. Simplified model of system to design H_∞ controller

The controller section C2M (see *Figure 4.5*) is composed of the plant controller, motor controller and motor. The H_∞ controller is designed for the remaining plant [19]. Once the C2M system model is obtained, the motor and controller model is separated from it leaving behind the controller for the plant. H_∞ controller provides more robust control hence it is used instead of a normal PI controller.

Motor Disturbance Torque Observer (F)

The disturbance torque observer is designed by using the methods explained in *Chapters 2* and *3*.

4.3 Road Torque Estimation

From *equation 4-2*, it is seen that the signal values required to reconstruct the torque sensor signal are torque on motor shaft, T_d and road reaction torque, T_{road}. The motor observer gives an estimate of the torque on motor shaft. The vehicle dynamic model is used to estimate the road torque [12, 20]. The road reaction torque itself is composed of different components. The major component of road torque which affects the steering is the tire aligning moment. The higher frequency components of road torque are neglected, so that it does not produce steering vibrations for the driver.

The vehicle dynamics equations and the various signals available from the other systems in the vehicle such as the Inertial Navigation System (INS), Electronic Stability Program (ESP), used for vehicle stability and Global Positioning System (GPS) are utilized to estimate the road torque, T_{road}. These systems communicate with each other using Control Area Network (CAN) bus.

Forces and moments from the road act on each tire of the vehicle and influence the dynamics of the vehicle. The force the tire receives from the road is assumed to be at the center of the contact patch between the tire and road and can be decomposed along the three axes as shown in *Figure 4.6*. As seen in *Figures 4.6* and *4.7*, it is the lateral force, F_y and the aligning moment, M_z which affects the orientation of the wheel and thus the direction of the vehicle. The lateral tire force is proportional to the slip angle, the angle between the orientation of the tire and the orientation of the velocity vector of the wheel, for small slip angles. The lateral tire force versus slip angle is shown in *Figure 4.8.*
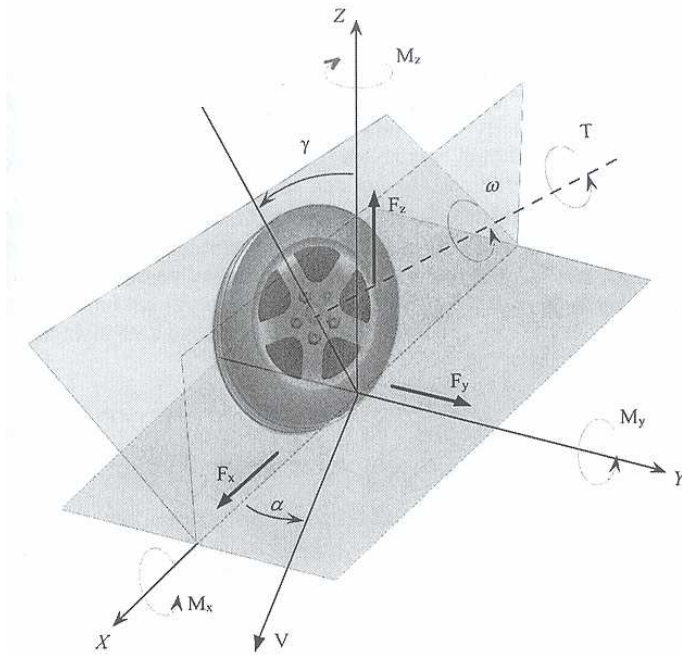
Figure 4.6. Tire forces and moments[1]
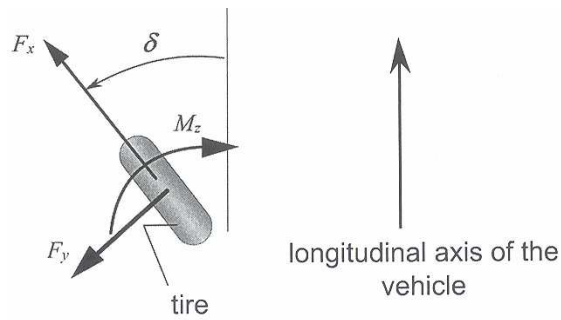

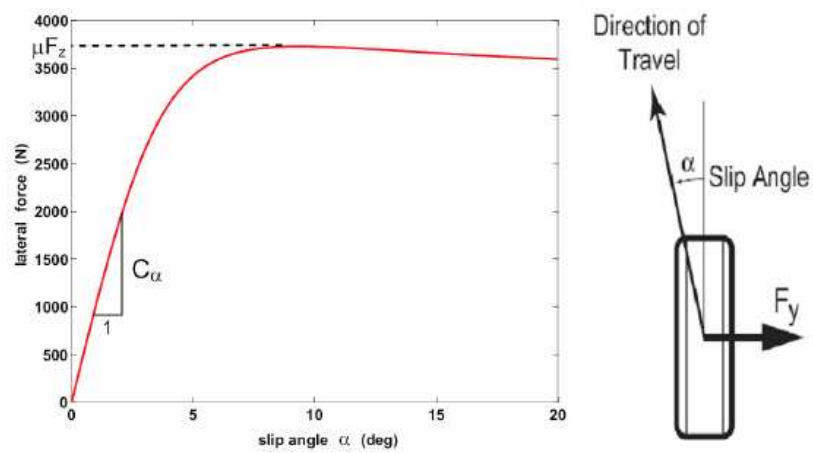*Figure 4.7. Relation between steering angle and the forces acting on the tire[1]*

Figure 4.8. Lateral force vs slip angle[1]

---

[1] Reprinted from "Vehicle Dynamics and Control", by Rajesh Rajamani, Springer,2005[20]

The linear operating region of the tire deformation can be modeled as

$$F_y = C_\alpha \alpha$$

(4-15)

The proportionality constant, C_α is called the cornering stiffness. C_α is a property of the tire and is mostly independent of the amount of tire grip available, which depends on the coefficient of friction between the road and tire, μ. It is seen from *Figure 4.8* that as the slip angle increases to higher values, the lateral force begins to saturate. That is if the vehicle is maneuvered aggressively, the lateral force saturates due to limited friction between tire and road surface, resulting in the loss of control over the vehicle. In the worst case of a completely frictionless surface, the direction of travel does not change even when the wheels are turned, as the lateral force does not change.

The total aligning torque is proportional to the lateral force by the distance the force is applied from the steering axis, known as the total trail. The trail is a function of the mechanical trail t_m, as well as the pneumatic trail t_p. The pneumatic trail is the distance between the resultant point of application of lateral force and the center of the tire and it depends on front slip angle α_f and the two tire parameters $C_{\alpha f}$ and μ. Mechanical trail is the distance between the tire center and the steering axis and is a constant function of steering geometry. For small slip angles it is seen that t_p can be considered as a constant too.

Thus, total alignment torque which tends to bring the wheels to center position is

$$T_{align} = -\left(t_p + t_m\right) F_{y,f} = -\left(t_p + t_m\right) C_{\alpha f} \alpha_f$$
$$= -t_0 \left[\frac{V_y + l_f \dot{\psi}}{V_x} - \delta\right]$$

(4-16)

where $t_0 = (t_p + t_m) C_{\alpha f}$. Thus the tire aligning component of road torque is obtained from the vehicle parameters and the tire slip angle. The tire slip angle is calculated

from vehicle velocities and yaw rate. These signals can be obtained from the INS which is used for vehicle stability systems. The accelerometer and gyroscope measurements from the INS are integrated to obtain V_y, V_x and $\dot{\psi}$.

$$V_y = V_y(0) + \int a_y dt \tag{4-17}$$

$$V_x = V_x(0) + \int a_x dt \tag{4-18}$$

$$\dot{\psi} = \dot{\psi}(0) + \int \ddot{\psi} dt \tag{4-19}$$

The motor shaft position signal, θ_m is then used to obtain the steering angle δ.

$$\delta = (n_s n)\theta_m \tag{4-20}$$

However, integrating the gyro and accelerometer measurements, $\ddot{\psi}$, a_y and a_x results in drifting yaw rates and velocities which can be avoided by using high speed, precise rotational equipment, which is very expensive. As cost is an issue in the automotive industry, this problem can be solved by using a cheaper two antenna GPS system. Absolute measurements of the slip-side angle, β can be obtained from the GPS which can be used to calculate the lateral velocity and yaw rate.

The slip-side angle is defined as the difference between the vehicle yaw angle, ψ and angle made by the velocity vector, γ. Both these values are measured in a two antenna GPS.

$$\beta = \gamma - \psi \tag{4-21}$$

$$\beta = \tan^{-1}\left(\frac{V_y}{V_x}\right) \tag{4-22}$$

$$V_x = |V|\cos\beta \tag{4-23}$$

$$V_y = |V|\sin\beta \tag{4-24}$$

where $|V|$ is the absolute velocity of the vehicle.

The vehicle yaw rate is obtained directly from differentiation of the GPS yaw angle.

$$\dot{\psi} = \frac{d}{dt}\psi \tag{4-25}$$

The GPS signals from *equations 4-21* to *4-25* could be used exclusively to calculate the tire slip, however, the refresh rate of GPS signals is slow, about 5Hz, thus making it insufficient for vehicle stability control or EPS application. Thus the GPS signals are used to update the values of the faster INS signals periodically in order to correct the integration drift.

CHAPTER 5

EXPERIMENTAL RESULTS

5.1 Hardware in Loop Configuration

Hardware in Loop (HIL) testing is used to check the performance of a system design subject to real world loads and disturbances. The designed model could also be tested in extreme conditions to see how well it retains its desired performance under those conditions. In HIL simulation, only the designed system is composed of hardware parts, the remaining plant dynamics are provided by software. This testing helps in obtaining the required data before implementing the designed model in an actual system thus saving cost and time taken to test the efficiency of the design. It is also suitable in cases where testing the design in the entire system is not feasible due to physical constraints and safety reasons.

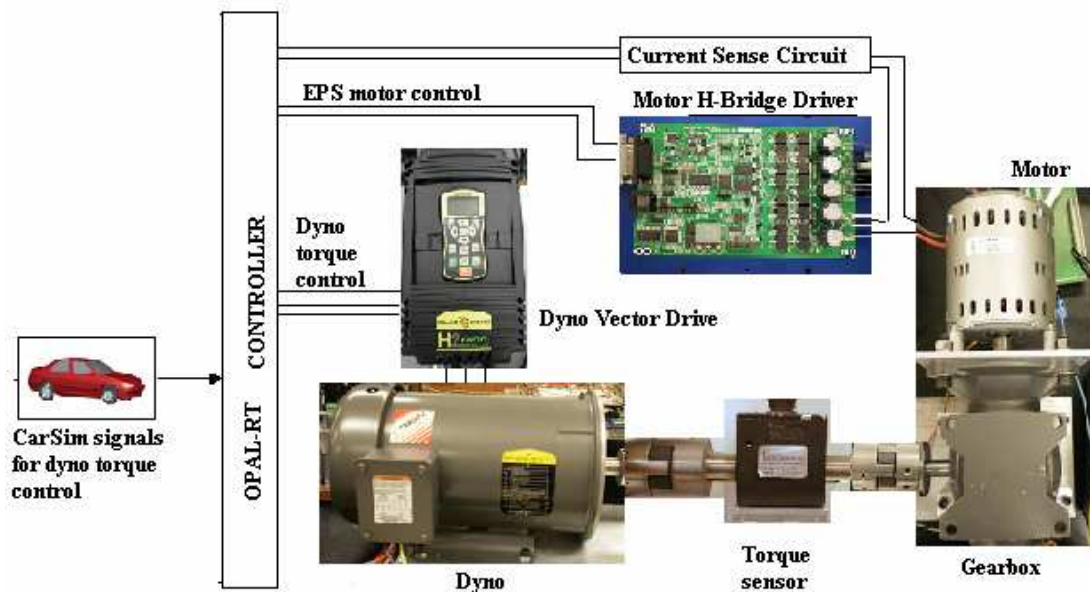The HIL test bench setup to test the proposed design is shown in *Figure 5.1*.

Figure 5.1. HIL test bench configuration

The test bench was set up for the general motor disturbance torque estimation experiment; at the same time considering the torque requirements in the EPS case study. For this purpose high torque DC motor was used as the test motor and a high torque Induction motor capable of delivering the actual road torque was selected as the dyno.

5.1.1 DC Motor

A 12V, 50 A, 400W Bosch DC motor is used as the test motor. The motor has a nominal torque rating of 1.2Nm. A gearbox is attached to the motor shaft to provide more torque to the load.

The model of the motor is complete only when the parameters of the motor such as R_a, L_a, J_m, B_m, K_t and K_v are available. These parameters are the design parameters which shape the performance of the motor for different applications. For example a low resistance, relatively high K_t motor indicates a motor which has high current and torque capacity. A motor with low viscous friction B_m will be able to attain higher speed limits. Most of the motors available in the market have these parameters available in their documentation. But some motors which are designed for specific purposes such as motors used in automotive industry do not have these parameter values available and it is required to determine these values to obtain the complete motor model to design the observer.

Method to determine DC motor parameters

Armature Resistance

A small voltage, V_t is applied to the motor terminals and the rotor is blocked. The current through the motor, I_a is measured using a shunt resistor. The readings are

taken once the current reaches steady state quickly as the rotor may heat up slightly causing the resistance to change.

$$R_a = V_t/I_a \tag{5-1}$$

Armature Inductance

A low amplitude sinusoidal voltage of frequency, ω_f is applied to the motor terminals and the rotor is blocked. The current is measured and plotted comparing it with the applied voltage. The lag between the two variables is measured and the phase lag angle, ϕ is calculated from the voltage and current plots shown in *Figure 5.3*.
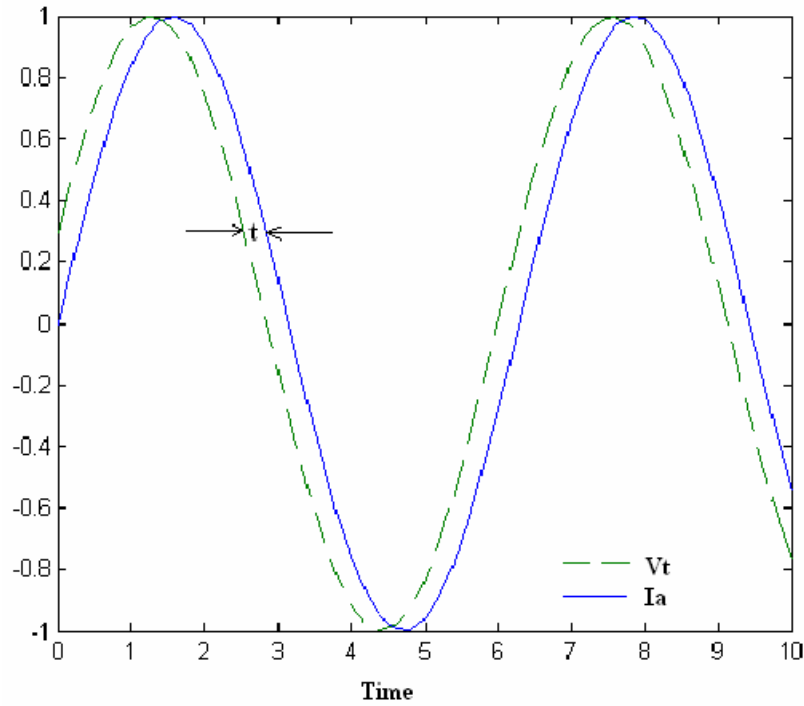

Figure 5.2. Applied Voltage and measured motor current plots to determine lag angle.

The phase lag angle is calculated from equation 5-2.

$$\frac{t}{T_{sine}} = \frac{\phi}{2\Pi}, T_{sine} \text{ is the time period of the sine wave.} \tag{5-2}$$

$$\tan(\phi) = X_L / R_a \longrightarrow L_a = R_a \tan(\phi)/\omega_f \tag{5-3}$$

An alternative method would be to measure the current amplitude, I_a and the applied voltage amplitude, V_t.

Impedance, $Z = V_t/I_a$ (5-4)

Inductance $L_a = \dfrac{1}{\omega_f}\sqrt{Z^2 - R_a^{\,2}}$ (5-5)

Electrical Constant and Mechanical Constant

In a DC motor, the electrical constant, K_v (V/rad/s) is equal to mechanical constant, K_t (unit Nm/A). The motor is operated at low steady state speeds and the voltage, V_t, current, I_a and speeds, ω are measured.

$$K_v = \frac{V_t - I_a R_a}{\omega}$$ (5-6)

$$K_t = K_v$$ (5-7)

This value of K_t could be checked by applying a small voltage to the motor and then determining the minimum amount of torque required from the dyno to block the motor. The current, I_a and the minimum dyno torque, T_D for blocked rotor condition is noted.

$$K_t = \frac{T_D/n}{I_a} \; ; \; n \text{ is the gearbox ratio}$$ (5-8)

Viscous friction constant

The voltage applied to the motor is increased in steps and the speed, ω and current, I_a are measured at steady state conditions.

$$K_t I_a = B_m \omega + K_f$$ (5-9)

By linear regression, B_m and K_f may be determined.

Inertial Constant

A step voltage is applied to the motor to run the motor at rated speed. The mechanical

time constant, t_M is measured.

$$J = t_M * B \tag{5-10}$$

Each experiment is repeated 2-3 times and the average taken to get more accurate values.

5.1.2 Motor Controller Configuration

The motor controller system is shown in *Figure 5.3*. A PWM controlled H-Bridge driver board is used for bi-directional control of the motor. The shunt resistor, R_{shunt} used for current sensing is connected in series with the motor. The motor controller used in this case has a current sensing circuit for protection purposes; however, the current measured by it is the current flowing from the power source to the driver board which is not equal to the motor current due to the PWM control (Appendix B). So when a PWM motor driver board is used, the circuit shown in *Figure 5.1* is used to measure the current magnitude and direction. Since the shunt resistor has very small resistance in the order of milliohms, an amplifier circuit is needed to amplify the voltage drop across the shunt resistor. An instrumentation amplifier is used for this purpose. The output voltage of the amplifier is proportional to the current flowing through the motor, and its polarity changes as the current direction switches. An instrumentation amplifier is preferred over an op-amp as it has better noise rejection with high Common Mode Rejection Ratio (CMRR). The measured current is sent through a low pass filter to remove white noise (Appendix C) to obtain a better current profile.

The measured current is given by *equation 5-11*.

$$I = \frac{V_o}{G \cdot R_{shunt}}, \tag{5-11}$$

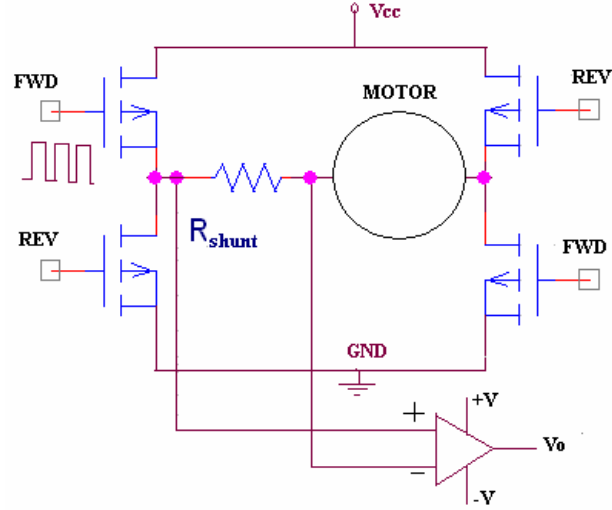V_0 is the instrumentation amplifier output, G the amplifier gain.

Figure 5.3. Current Sensing in a PWM controlled H-Bridge PWM motor driver circuit

The relation between the analog control input, V_{in} to the driver board and its output, V_m is used to determine the voltage applied across the motor.

$$V_m = -4.8V_{in} + 12 \tag{5-12}$$

V_{in} is the control signal sent by the Opal-RT. V_m is used by the disturbance torque observer in its computations.

5.1.3 Dyno Motor

A 5hp, 3 phase, 240V, 22A Baldor Induction motor is used as the dyno. The full load torque rating of the motor is 20.18Nm. An AC motor is selected because the load torque requirement is quite high; about 20Nm. Using a DC motor for such high torque would require a bigger machine with higher power requirements. Considering the space, power and performance issues, a 3 phase induction motor is selected to simulate high load torque.

5.1.4 Dyno Controller Configuration

A vector drive is used to control the torque of the dyno. The configuration used by the dyno controller is as follows

Operating Mode: Bipolar, Open loop vector mode

Operating zone: Quiet variable torque, 8kHz PWM (Appendix C)

Command source: Analog Input 2

Analog Input 1: Current Limit source, 0 to 10V

Analog Input 2: Torque signal, -10V to +10V

The drive control is operated by the opto-isolated digital inputs J2-8 to J2-20 shown in *Figure 5.4* .The opto inputs can be switches or logic signals. Transistors were used in this case to switch the inputs on and off in this case, as it can be controlled by analog signals from Opal-RT.
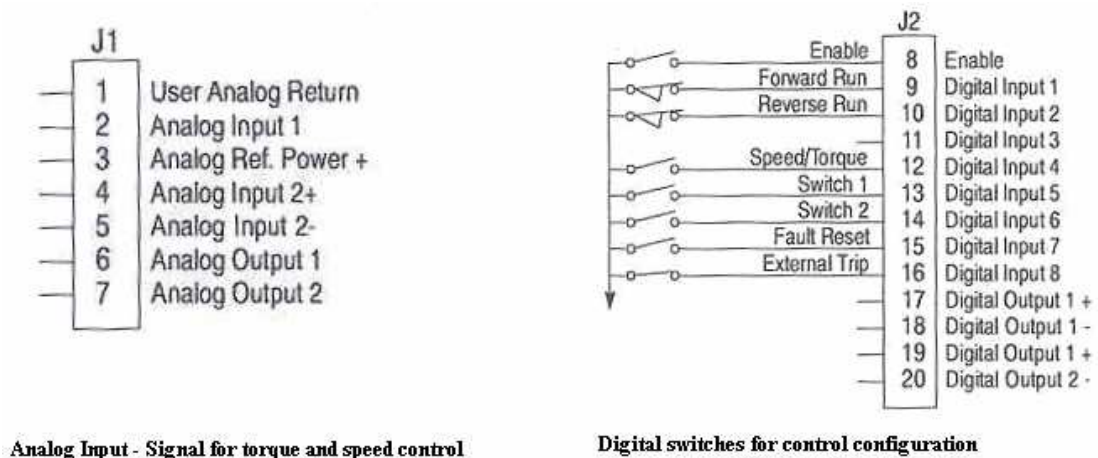

Figure 5.4. Dyno driver control inputs

The torque in the dyno is controlled by analog input 2 and the direction is controlled by the digital switches FWD and REV. For positive torque, a +ve signal is sent through Analog 2 and the direction is selected as FWD. For negative torque, a –ve signal is sent through Analog 2 and the REV direction is selected. The relation between the control signal, V_2 sent to the dyno and the torque, T (in Nm) is

$$T = 3.6V_2 + 0.036 \qquad\qquad (5\text{-}13)$$

The model used for dyno torque control is shown in *Figure5.5.*
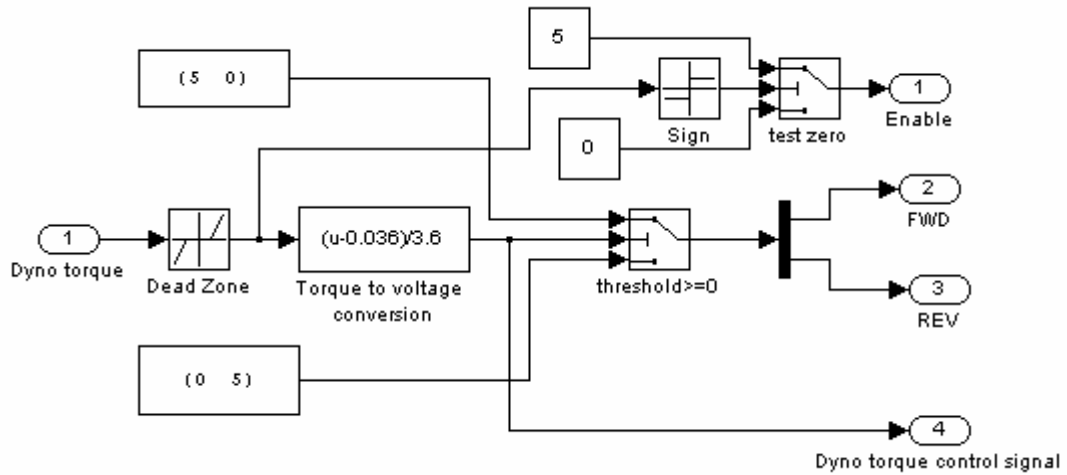
Figure 5.5. Dyno control block in Simulink

5.1.5 Gearbox/ Speed Reducer

As high torque, low speed is required at the load end, a speed reducer is used. A 20:1 ratio Baldor speed reducer is used to amplify the motor torque to sufficient levels. The speed reducer is designed such that the torque flow is permitted in only one direction from high speed side (input) to low speed side (output). This design is for safety reasons to ensure that the load does not drive the input under any condition. The specifications of the speed reducer are given in Appendix A.

5.1.6 Torque Sensor

A torque sensor is used to validate the estimation results of the designed disturbance torque observer. The torque capacity of the sensor is 56 Nm and is capable of withstanding 150% overload. The sensor specifications are given in Appendix A.

The sensor operates as any other strain gage sensor, providing mV/V output for torsional force. When the motor is operated with no load torque acting on the gearbox shaft, i.e., dyno in off condition, the output of the sensor is zero as there is no torisonal force on the torque sensor shaft. When a dyno torque is applied to the gearbox shaft during the motor operation, the torque measured by the torque sensor divided by the gearbox ratio gives the disturbance torque acting on the motor shaft. This signal is compared with the observer torque signal. However when the dyno torque exceeds the blocking torque of the motor, this additional torque is not reflected on the motor shaft and under these conditions, the disturbance torque estimate would differ from the measured torque sensor value. Due to the gearbox design of unidirectional torque flow, further increase in dyno torque, does not reflect on the input side of the gearbox, i.e, the motor shaft, while it continues to act on the gearbox output shaft. As the torque sensor is connected between the dyno and gearbox, this torque is measured by the torque sensor.

The torque sensor also includes an encoder with a resolution of 512ppr. To measure high speeds, the sampling time of the measuring device, i.e., Opal-RT analog input, is made small enough to count each pulse.

5.1.7 Opal-RT Configuration

The Opal-RT is configured to run at 1ms step size and the data is stored by using the Opwrite data logging block. The Opal-RT is capable of maintaining real-time computation upto step size 250μs. A step size lower than 250μs causes the computation to slow down, affecting the HIL setup. Algebraic loops are not permitted in Opal-RT computation, so a data store memory block is used to store the estimated torque data, from which the data is then read during the computation.

5.1.8 EPS Case Study- CarSim Configuration

CarSim provides the vehicle dynamics data to simulate the load torque on the EPS motor shaft and also the signals used to compute the road torque to be used for torque sensor signal estimation. The input and outputs used by the CarSim block is shown in *Figure 5.6.*
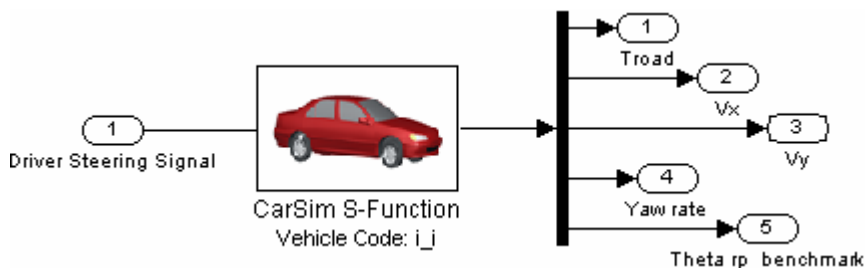

Figure 5.6. CarSim block input and output parameters

The input to the CarSim block, the driver steering signal may be configured as steering wheel angle or torque. When it is required to use torque as input to CarSim block, the OPT_STEER parameter must be set as 1 in the Over-riding data block after checking the "More" box as shown in *Figure 5.7*. Other parameters such as column and rack inertia and viscous friction coefficients can also be set to user defined values in this block.

The outputs of the CarSim block are taken as the left and right wheel steer which is used to obtain the pinion benchmark, the road reaction torque to be used by the dyno controller, yaw angle, longitudinal and lateral speed for computing the road torque to be used by the FTC controller to estimate the torque sensor torque.
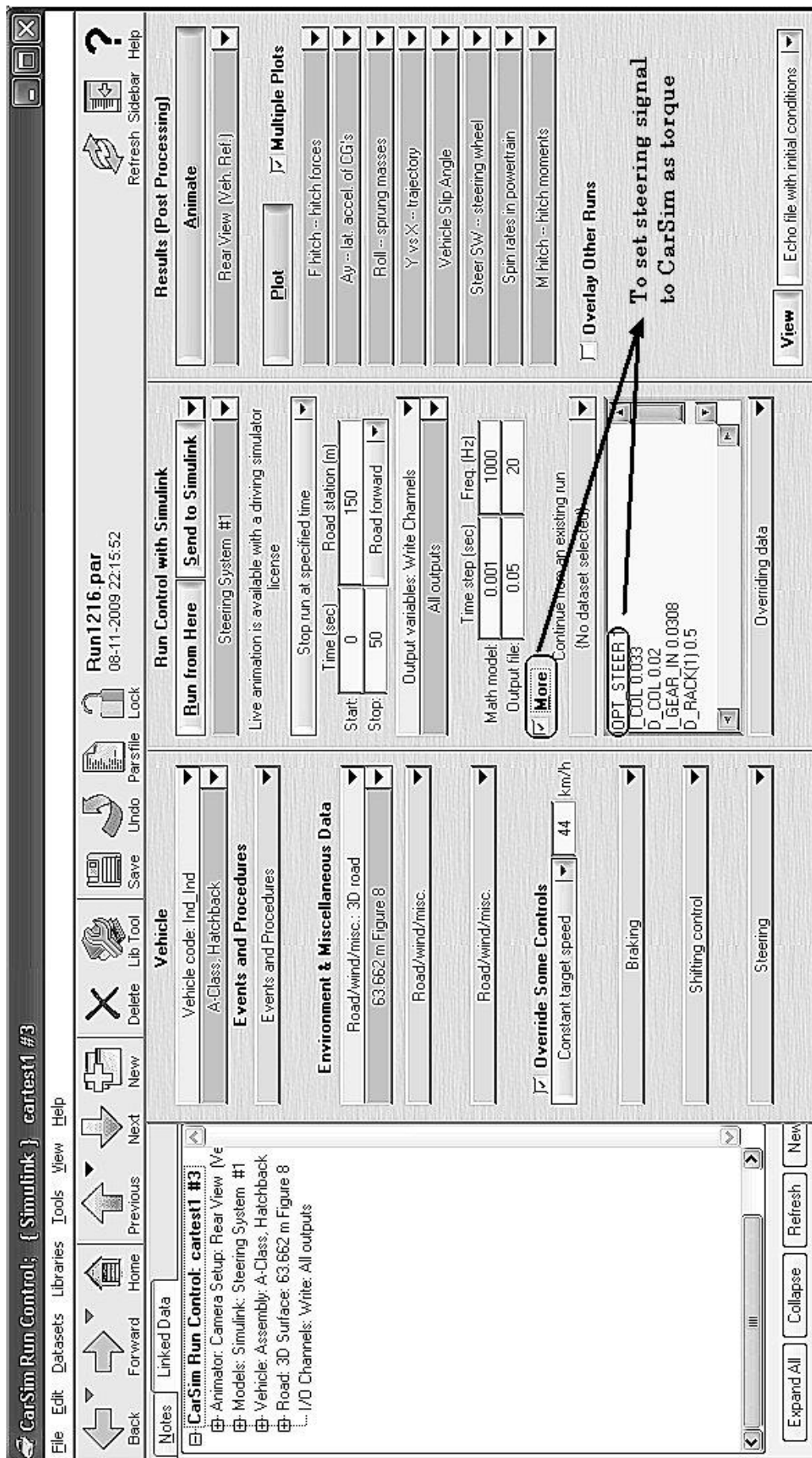
Figure 5.7 CarSim Window to set Run conditions

5.2 RESULTS

The HIL results for load torque estimation are shown here. The performance of the observers discussed in *Chapters 2* and *3* are compared. Measured T_d is the data obtained from the HIL test bench torque sensor, reflected on the motor shaft side.

Test 1: The motor current is controlled by applying a reference current profile as shown in *Figure 5.8*, and the controlled dyno torque is shown in *Figure 5.9*.
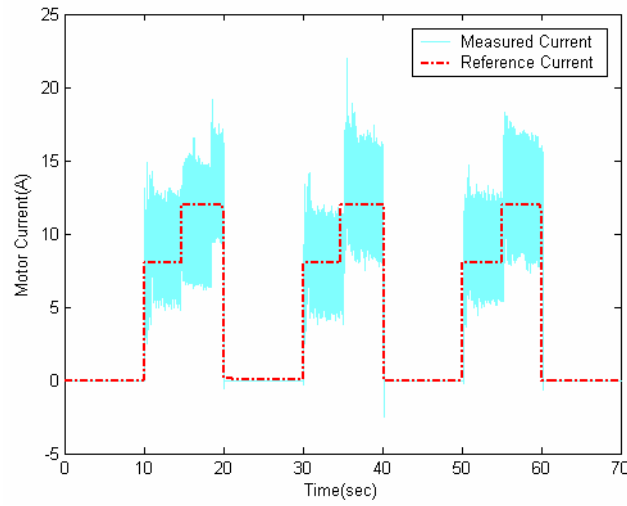

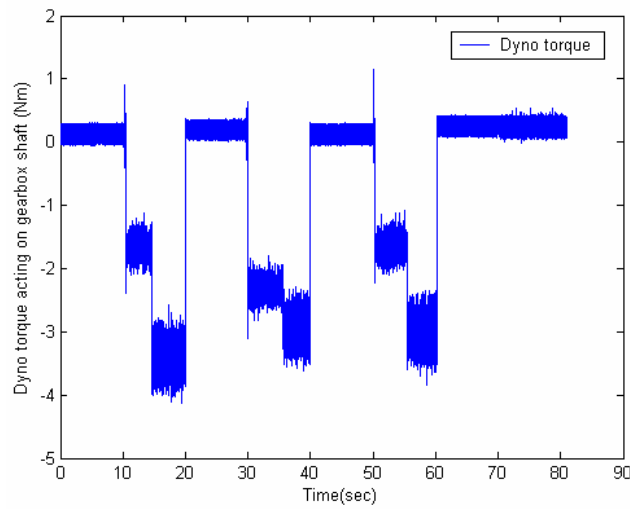*Figure 5.8. Motor current-test 1*

Figure 5.9. Dyno torque-test 1

Case 1: Load torque estimation with nominal parameters used for observer design.

The estimated load disturbance torque is shown in *Figures 5.10, 5.11* and *5.12*. The disturbance torque estimate using Luenberger filter is shown in *Figure 5.10*. It is seen that the system noise affects the estimate, with the estimated signal having more noise than the measured torque sensor signal. The H_∞, H_∞ Gaussian and Kalman filters are compared in *Figure 5.11*. The weights used in the uncertainty matrix B_1(*equations 3-6 ,3-9*) are $w_1=1$, $w_2=0.1$. The magnified view of the estimates from 30 sec to 40 sec is shown in *Figure 5.12*. It is seen that the difference between the 3 filters' estimates is very low, about 0.02 to 0.05.
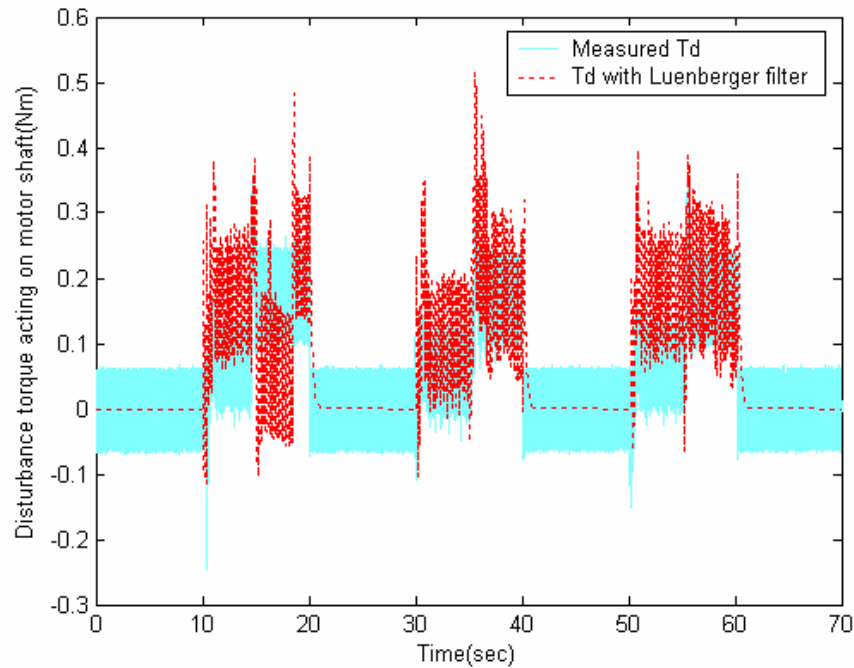

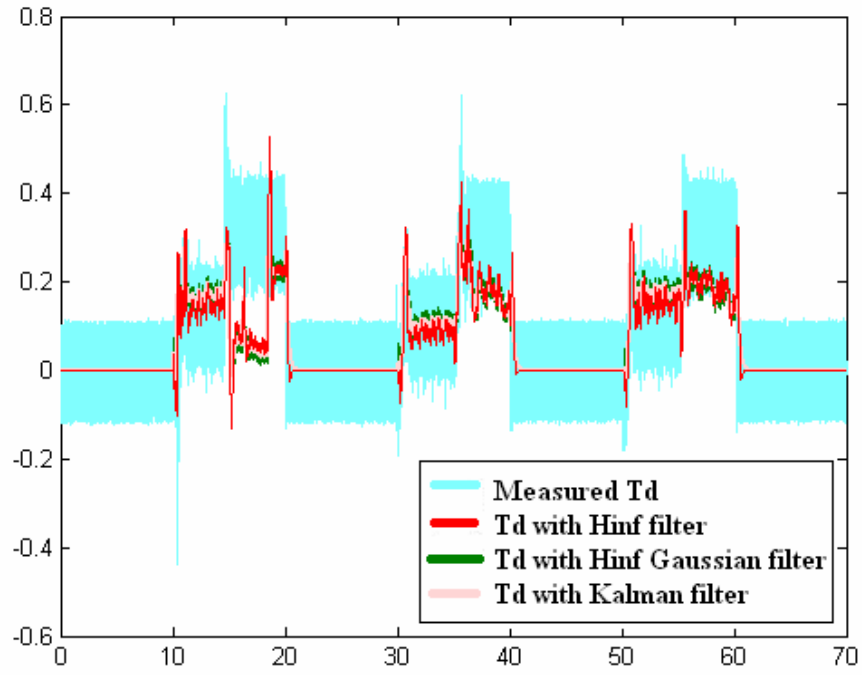*Figure 5.10. Estimated disturbance torque using Luenberger filter- test 1, case 1*

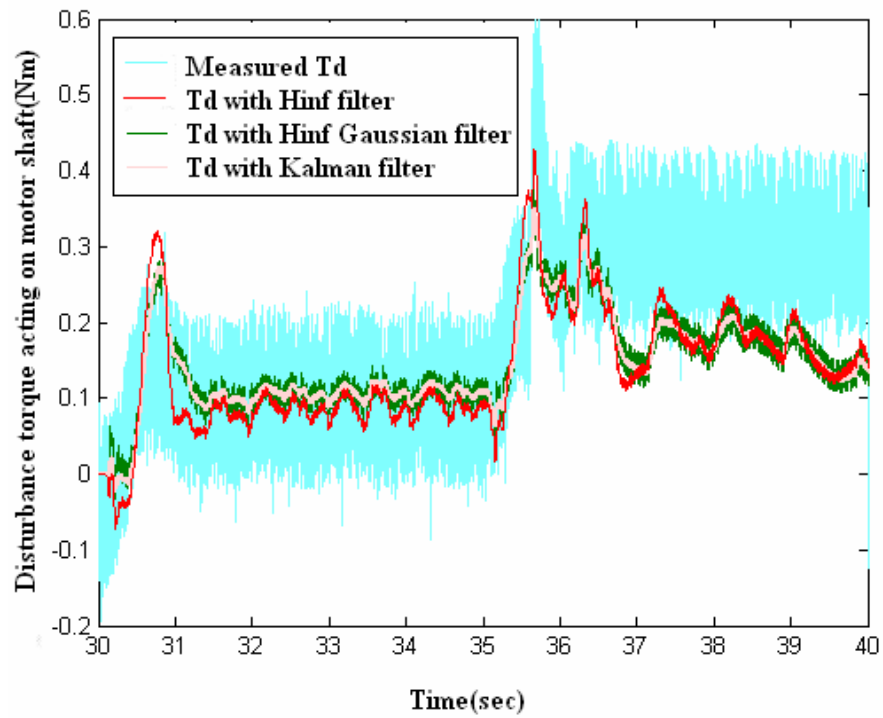*Figure 5.11.Estimated disturbance torque - test 1, case 1*

Figure 5.12. Magnified view of estimated disturbance torque from 30 to 40sec

Case 2: Load torque estimation with 20% parameter uncertainty in motor resistance.

The weight matrix of uncertainty vector is varied to understand the significance of the weights on observer performance.

It was observed that the Luenberger observer becomes unstable in these conditions. The performances of the remaining 3 filters are compared in *Figure 5.13*. It is observed that there is no difference between the H_∞ Gaussian filter estimate and the Kalman filter estimate. While designing the H_∞ Gaussian filter, a high value of γ, (the design parameter used in H_∞ and H_∞ Gaussian filter), was required for stable conditions. This makes the H_∞ Gaussian filter approach Kalman filter performance. The weights in B_1 matrix are changed and the filter performance observed in *Figures 5.14* and *5.15*.

It is seen that as the weight assigned for the disturbance torque reduces, lower value of γ is required for stable conditions. It is observed that the set of weights $w_1=1,w_2=0.1$ gives the best performance for H_∞ filter as when the weight w_2 is lowered further, though less noise is observed in the estimate, the estimation delay is found to increase. Lowering the weight w_2 has an effect of increasing the inertial constant of the model used by the observer, thus increasing the response time of the observer to the disturbance torque.
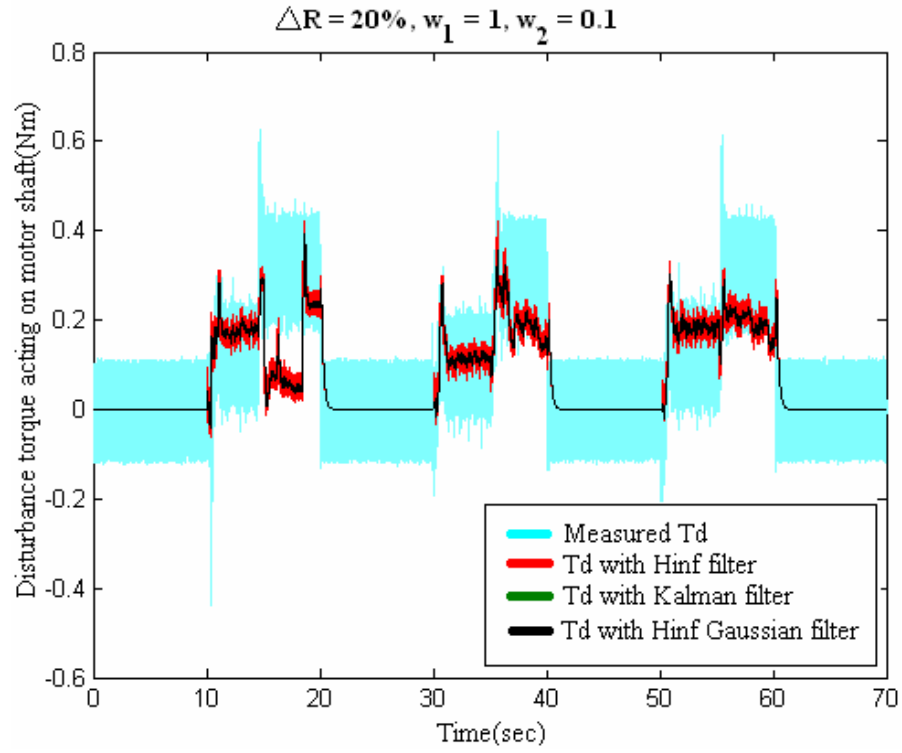
Figure 5.13. Estimated disturbance torque - test 1, case 2, $w_1=1, w_2=0.1$.
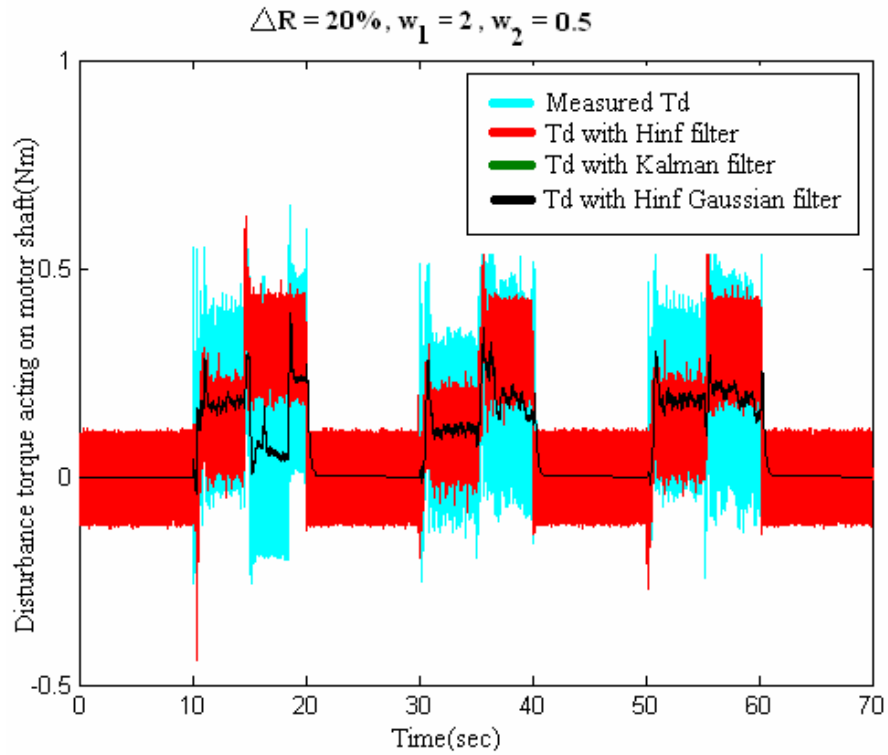
Figure 5.14. Estimated disturbance torque - test 1, case 2, $w_1=2, w_2=0.5$
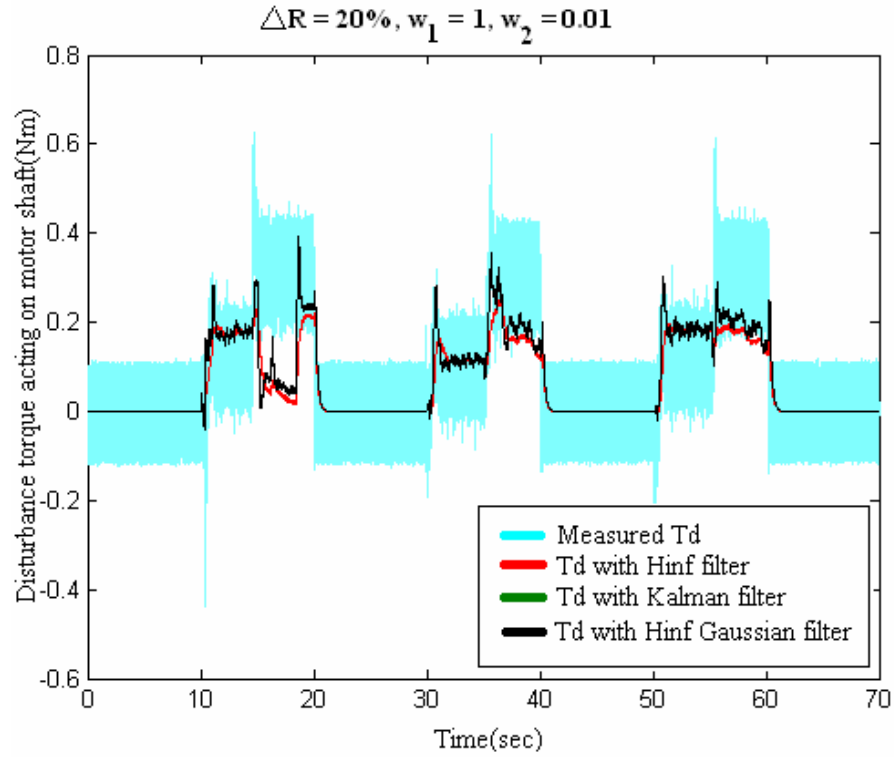
Figure 5.15. Estimated disturbance torque - test 1, case 2, w_1=1, w_2=0.01.

Case 3: Load torque estimation with observer design for 40% model uncertainty.

The resistance uncertainty is considered to be 40% while designing the observer.

The estimates using H_∞, H_∞ Gaussian filter and Kalman filter are compared in Figure 5.16. The H_∞ Gaussian plot and Kalman plot have the same performance as mentioned earlier.
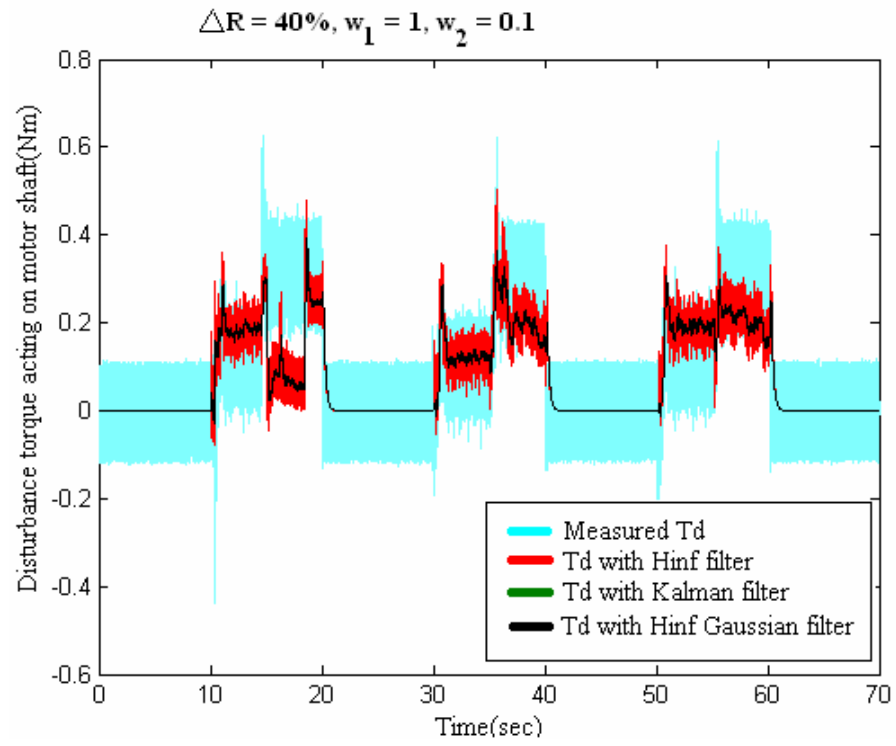
Figure 5.16. Estimated disturbance torque - test 1, case 3

Test 2: The motor current is controlled by applying a reference current profile as shown in *Figure 5.17*, and the controlled dyno torque is shown in *Figure 5.18*.

This test checks the performance of the observer with dynamic torque conditions. The H_∞ Gaussian filter is used and a parameter uncertainty of 20% in resistance, R_a is considered.
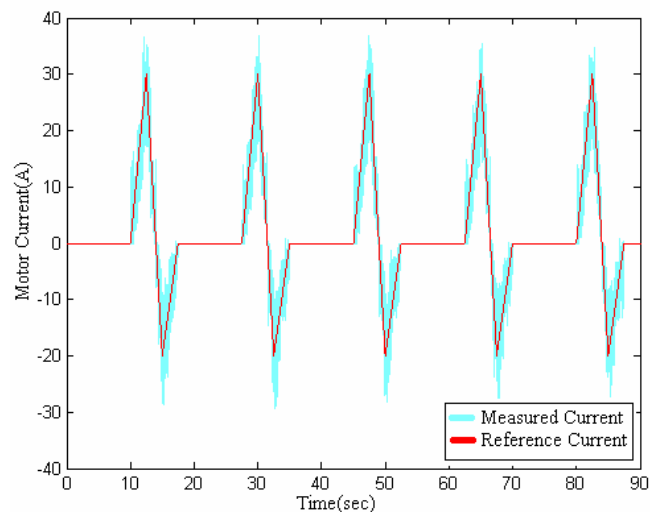
Figure 5.17. Motor current-test 2
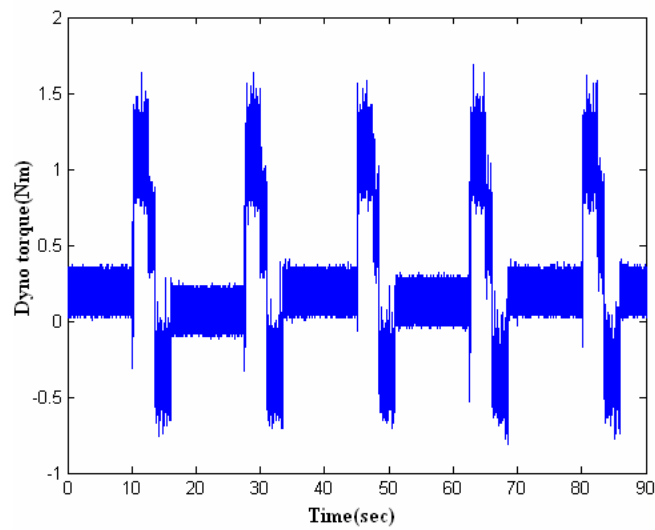
Figure 5.18. Dyno torque-test 2
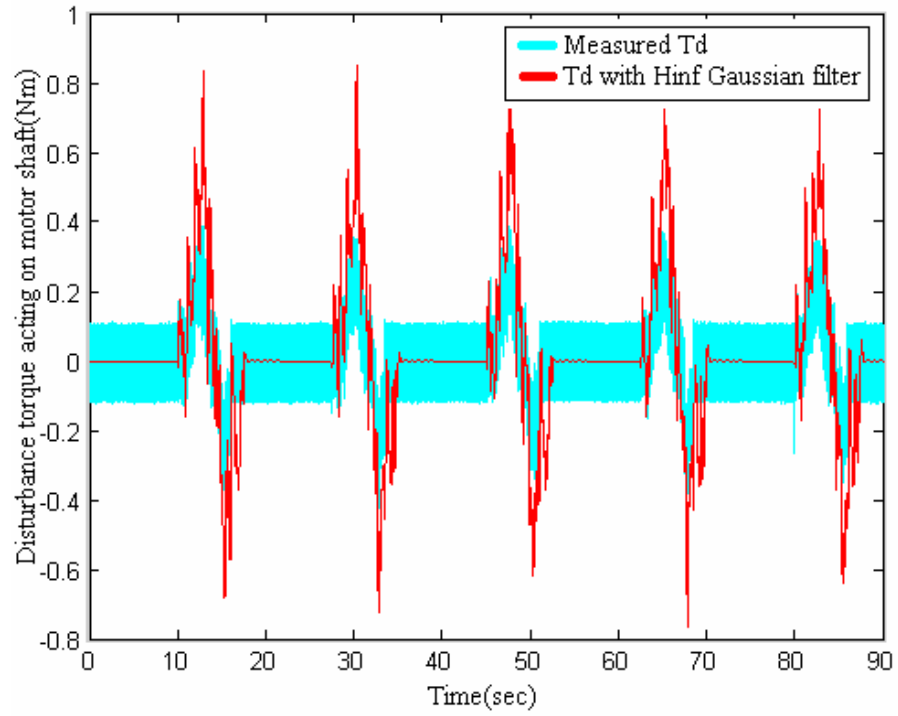
Figure 5.19. Estimated disturbance torque using H_∞ Gaussian filter- test 2

From *Figure 5.19*, it is evident that the observer gives good performance with dynamic torque conditions thus making it suitable for all torque conditions- steady state or dynamic.

Test 3: Fault tolerant control of EPS- HIL results

Load torque estimation based fault tolerant control is done for the EPS case. The test data for EPS case is given here. The driver steering torque is shown in *Figure5.20*. A constant vehicle speed of 44km/hr is considered. The H_∞ Gaussian filter is used and a parameter uncertainty of 40% in resistance, R_a is considered.
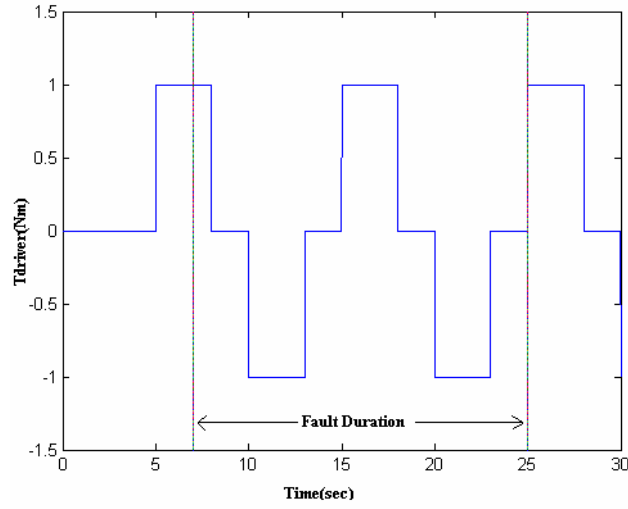
Figure 5.20. Driver steering torque

The torque acting on the motor shaft and the estimated torsion bar torque are shown in *Figure 5.21 and 5.22* respectively.
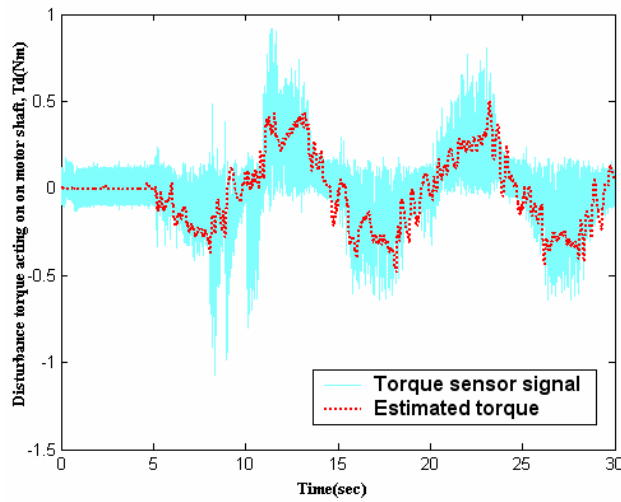
Figure 5.21. Disturbance torque acting on motor shaft
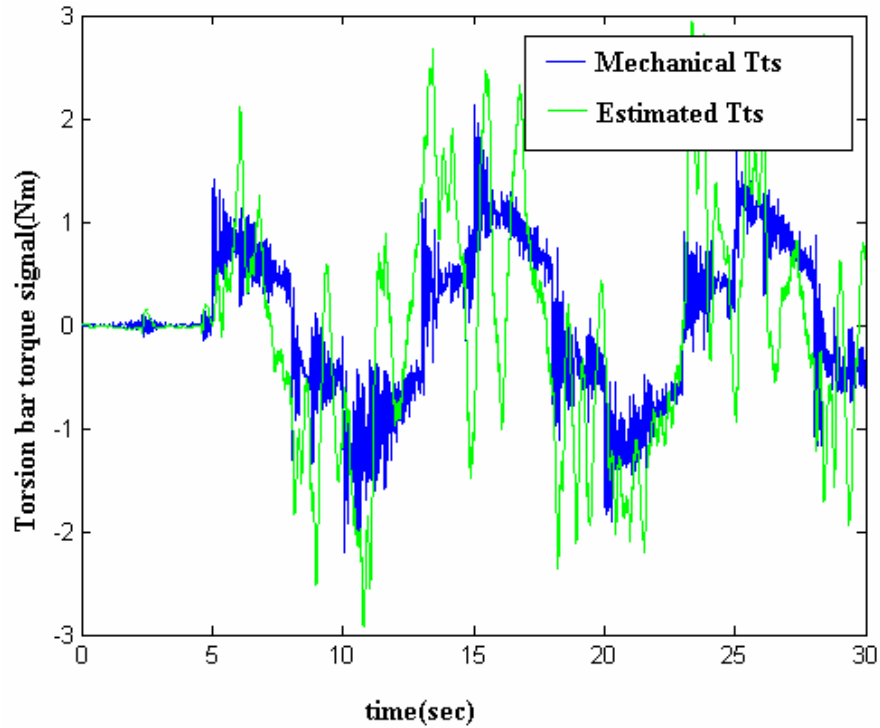
Figure 5.22. Torsion bar torque signal

The estimated torsion bar torque tracks the actual torque fairly well, with some spikes caused due to external noise. So in this case two thresholds are used in the FTC-upper and lower thresholds. The lower threshold, *Kl* is used to switch to estimated sensor signal when a fault is detected and the upper threshold, *Ku* is used to switch back to measured value, when the estimated signal has spikes. The controlled pinion angle with *Kl*=0.6 and *Ku*=1.7 is shown in *Figure 5.23*. The FTC is tested with different threshold values to check the performance of the control as threshold is varied. The controlled pinion angle using different threshold values may be compared in *Figure5.24*. It is seen that the controlled pinion angle using FTC tracks the normal required pinion angle quite well. Some reasons for the difference in FTC controlled angle and normal angle for the duration 10-17sec could be the selection of threshold values. Also due to the gearbox design, there are instances when the applied dyno torque is not detected by motor observer, as explained in *Section 5.1.6*. This could cause an estimation error.
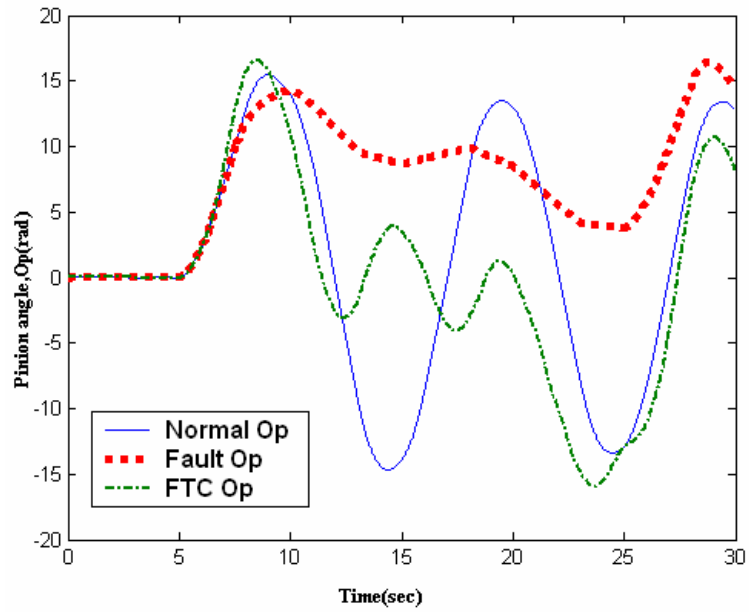
Figure 5.23. Pinion angle vs time, FTC with Kl=0.6, Ku=1.7

Figure 5.24. Pinion angle with FTC using different threshold values

Here normal Op is the controlled pinion angle when no fault occurs, fault Op is the pinion angle when fault occurs and FTC is not used, FTC Op is the pinion angle when fault occurs and FTC is used.

CHAPTER 6

CONCLUSION AND FUTURE WORK

A disturbance torque observer for a PMDC motor is designed taking into account the various disturbances acting on the system. While most disturbance torque observers are designed for steady state load conditions, the proposed disturbance torque observer works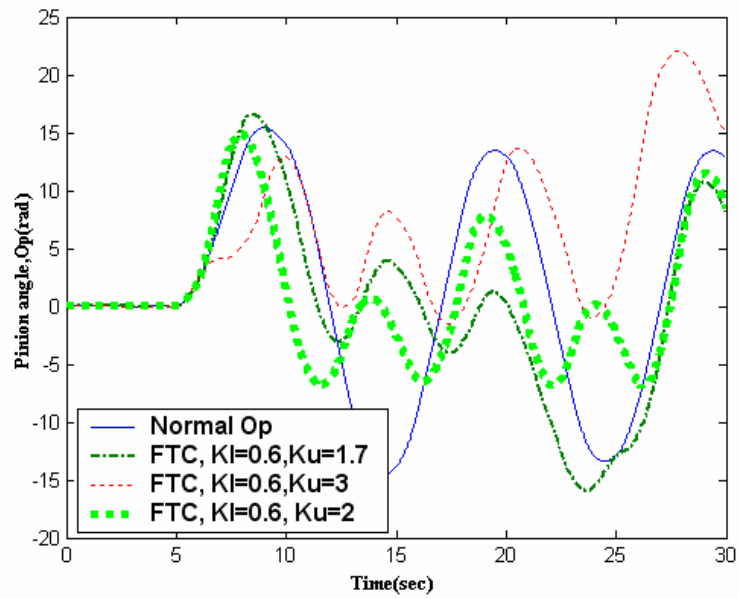 well with dynamic as well as steady load conditions, making it applicable in any system using motor as actuator. The state model construction plays an important role for observer design. The observer estimation accuracy is determined by how accurately the model is obtained.

The significance of different filter designs and their performance under different disturbance conditions are also studied. The Luenberger filter being designed for an ideal system model does not perform satisfactorily in real world cases where noise is an unavoidable occurrence. The Kalman filter is recommended when the model of the system is fairly accurate and good performance towards white noise is the requirement. For a low inertia motor with uncertain model parameters, an H_∞ filter is recommended for disturbance torque estimation. It is found that low motor inertia affects the design of H_∞ and H_∞ Gaussian filter. With lower motor inertia, smaller uncertainty limits are tolerated by the observer and controller to maintain stable conditions. The performance of the H_∞ Gaussian filter for a low inertia motor towards model uncertainty is poor. For a high inertia motor, an H_∞ Gaussian filter is recommended, as it is gives good performance towards white noise as well as model uncertainty.

Hardware in Loop testing with high current machines showed the vulnerability of the system to electromagnetic interference and harmonic noise. This reflected the real

world case where high currents flowing in nearby circuits could affect the control and estimation of the system under test. Methods to reduce the impact of electromagnetic interference on the system are also studied.

In this test bench, the gearbox permits torque flow in only one direction, i.e, from motor to dyno side. So only when the motor is switched on, some torque is detected on the motor shaft. When the motor is off, no torque acts on the motor shaft, irrespective of the magnitude of the dyno torque. Due to the same reason, a torque higher than the stalling torque of the motor is not detected by the observer. Using a gearbox which permits 2-way flow of torque would help detect the load torque in both, motoring and generating operation.

The significance of load torque estimation in FTC and the various factors which could affect the FTC performance are studied. When load torque estimation is used for fault tolerant control, the level at which the residual threshold is set is very crucial. Too low thresholds trigger the switching to FTC for small differences between estimated and measured torque which may not actually be a fault condition. At the same time, too high thresholds cause the switching to FTC to be very late, well after the fault has occurred, thus defeating the very purpose of FTC. The selection of thresholds is done by conducting experiments to check the range of measured and estimated sensor signal and also the range of error in estimates. In some cases, like the EPS case study taken in this research, two thresholds may be required, a lower and upper threshold to switch to estimated sensor signal and back to measured signal respectively. The upper threshold is used when external noise causes spikes in the estimated signal which could affect the fault tolerant control.

Future Work

   The performance of H_∞ Gaussian filter towards uncertainty in model parameters other than the motor resistance should be studied and the uncertainty limits tolerated by the filter for each parameter noted. This data could then be used to design a universal motor disturbance torque observer for a class of motors whose parameters are within the uncertainty limits tolerated by the filter.

   A systematic method to determine the set of weights on the uncertainties should be investigated to obtain the best performance of the filter. When arbitrarily chosen weights are used by trial and error method, the best performance of filter is not guaranteed. A method based on neural networks could be used to train the network to obtain optimized uncertainty weights for desired performance.

APPENDIX A

Test Bench Model Parameters and Specifications

Motor Parameters

Armature Resistance 0.165Ω

Armature Inductance   4.9mH

Electrical constant   0.02V/rad/s

Mechanical constant   0.02Nm/A

Inertial coefficient (Motor + Dyno) $0.00018kg/m2$

Viscous Friction coefficient (Motor + Dyno)   0.0005Nm/rad/s

Coulomb Friction (Motor + Dyno)   0.02Nm

Torque Sensor Specifications

Capacity   500in-lbs = 56Nm

Output @ F.S $\pm5V$

Non-linearity (%F.S.O)   0.1

Hysteresis (%F.S.O)   0.1

Overload (Torque)   150% F.S

Max Speed   10,000rpm

Power Input (Regulated)   12-15VDC (Min 11, Max 15.75VDC)

Current Draw (Max)   350mA

Position Encoder

Resolution   512 pulses/rev w/quadrature

Gearbox Specifications

Ratio   20:1

Max. Input Power   0.36hp

Max. Torque rating   220 in-lbs = 24.64Nm

Output rpm @ 1750   88 rpm

APPENDIX B

Current Sensing in a PWM motor driver board

The controller measures and limits the current that flows from the battery. Current that flows through the motor is typically higher in a PWM H-bridge motor driver[23]. This counter-intuitive phenomenon is due to the "flyback" current in the motor's inductance. In some cases, the motor current can be extremely high, causing heat and potentially damage while battery current appears low or reasonable.

The motor's power is controlled by varying the On/Off duty cycle of the battery voltage 16,000 times per second to the motor from 0% (motor off) to 100 (motor on). Because of the flyback effect, during the off time current continues to flow at nearly the same peak and not the average level as during the on time. At low PWM ratios, the peak current and therefore motor current - can be very high as shown in *Figure B.1.*
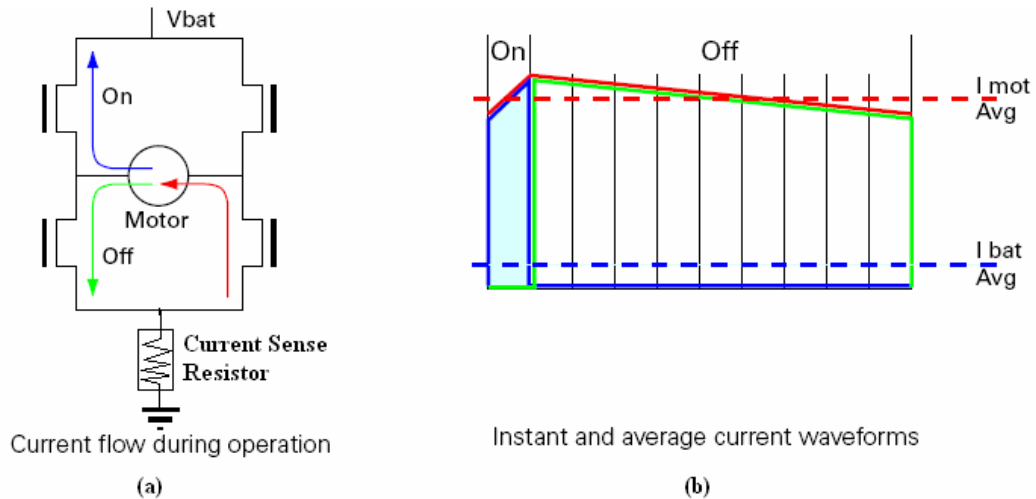

Figure B.1 (a) Current flow in PWM controlled H-Bridge (b) Instant and average current waveforms of power source and motor

The relation between Battery Current and Motor current is given in the formula:

Motor Current = Battery Current / PWM ratio

APPENDIX C

Noise Reduction in Motor Drives

Motor Signal Noise Reduction

The electrical noise in a PMDC brushed motor is due to the commutator and brush contact, shown in *Figure C.1*. At each commutation point, when the brush breaks contact with a commutator segment, the energy stored in the motor winding as a magnetic field causes an arc or voltage spike between the brush and the commutator segment. This occurs not only during normal commutation but also in situations where the brushes "bounce" on the rotating commutator. As the speed increases, the noise spectrum also increases. A method to determine the motor speed by observing the current noise is also available in [25].

Figure C.1. DC commutator and brush

For better data interpretation, the electrical noise may be suppressed by using an RC low pass filter at the output of the instrumentation amplifier before it is sampled by the Opal-RT controller. The difference in current waveform with and without filter is shown in *Figure C.2*.
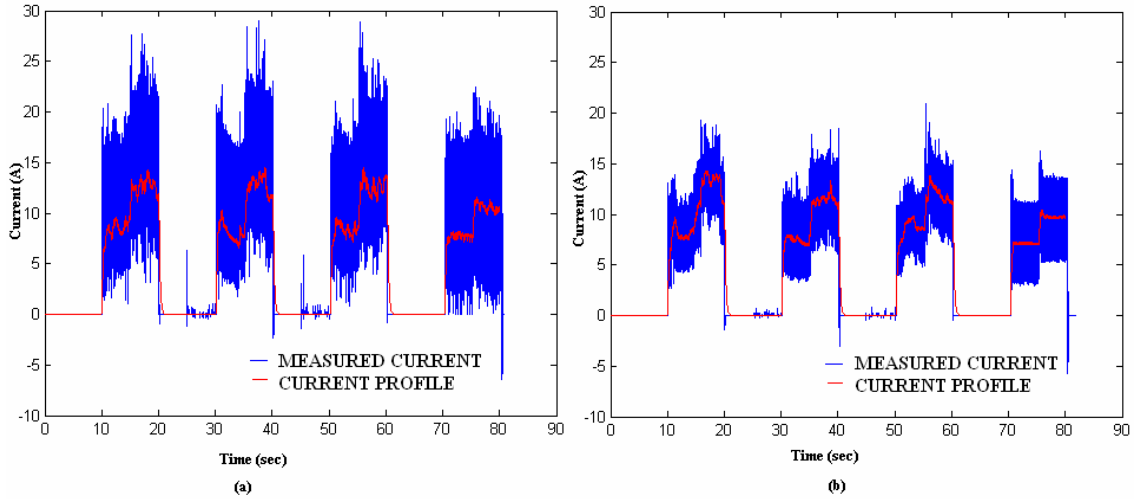
FigureC.2. Current waveform (a) without using filter (b) using RC low pass filter

As the sampling time of Opal-RT is 1ms, a cutoff frequency of 1 kHz was selected to design the RC low pass filter. With lower noise, better current control is obtained.

PWM controllers are another source of electromagnetic noise interference. PWM switching results in radiated noise from motor lead wires. Shielding and lead wire placement also help mitigate the effect of PWM generated EMI.

Harmonic Noise Reduction in Vector Drive

Most vector drives require minimum input line impedance in order to suppress the harmonics present in AC power. Harmonic noise is identified by the low humming produced when the motor is energized, and the periodic voltage spikes in the surrounding equipment. By operating the drive in Quiet Variable torque mode at 8 kHz PWM, the harmonic noise is reduced to some extent. Adding a load reactor to the setup further suppresses the noise and voltage spikes. Without a load reactor, harmonic currents produce voltage spikes in the surrounding electrical equipment disturbing the measurements used for control purposes as shown in *Figure C.3*.
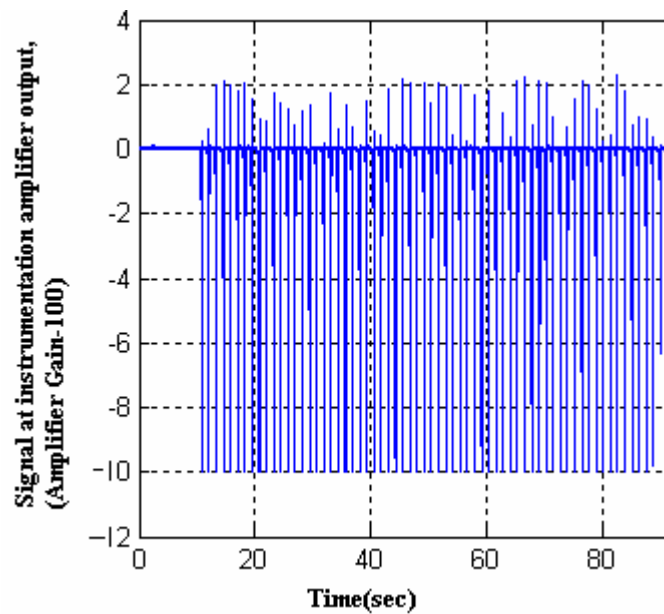
Figure C.3.Noise induced in current sensing circuit due to dyno currents.

The input impedance of the power lines can be determined as

$$\% \text{Impedance} = \frac{\text{Volts}_{\text{No Load}} - \text{Volts}_{\text{Full Load}}}{\text{Volts}_{\text{No Load}}} \times 100$$

A minimum of 1% impedance is required by the Baldor drive to operate satisfactorily.

The inductance of the reactor required for n% impedance is calculated as

$$L = \frac{V_{L-L} \times n/100}{I \times \sqrt{3} \times 377} \quad \text{for 60Hz power}$$

The recommended % impedance in typical applications is shown in *Table C.1*.

Table C.1 Recommended % impedance in typical applications

% Impedance	Typical Applications
3	Current surge protection, voltage transient protection, drive nuisance tripping, voltage notch reduction (SCR's), capacitor switching spike protection, motor short circuit protection, multiple motor applications
5	Harmonic reduction, motor temperature reduction, motor noise reduction, motor efficiency improvement, IGBT w/ long lead lengths

A 3% load reactor RL 02501 is used in this setup.

Methods to reduce noise

1. Shielded cables should be used for high power and sensitive equipment with the shield grounded.

2. Capacitors should be used at the power side of the instrumentation amplifier to ensure only filtered constant DC reaches the instrumentation amplifier.

3. All metal bodies in the setup should be grounded so that any voltage spikes induced by high currents are conducted to ground.

4. Keep wires as short as possible and remove any stray wires which may act as antenna.

5. Signal, power and motor cables should be separate and positioned independently of each other.

6. For reducing mechanical noise, a heavy metallic base should be used to mount the machines and the shaft alignment of the interconnected parts should be within permissible limits.

REFERENCES

[1] Giuseppe S. Buja, Roberto Menis, Maria Ines Valla; "Disturbance Torque Estimation in a Sensor-less DC Drive", IEEE Transactions on Industrial Electronics, Vol. 42, No.4, August 1995

[2] Hisao Kubota, Kouku Matsuse, " Robust Field Oriented Induction Motor Drives based on Disturbance Torque Estimation without Rotational Transducers", Industrial Applications Society Annual Meeting, 1992, Conference Record of 1992 IEEE, , Vol.1, 4-9 October 1992.

[3] Jorge Solsona, Maria. I. Valla, Carlos Muravchik, " Nonlinear Control of a Permanent Magnet Synchronous Motor with Disturbance Torque Estimation", IEEE Transactions on Energy Conversion, Vol.15, No.2, June2000.

[4] Ki-Hong Park, Tae-Sung Kim, Sung-Chan Ahn, Dong-Seok Hyun, " Speed Control of High Performance Brushless DC Motor Drives by Load Torque Estimation", Power Electronics Specialist Conference, PESC'03, 2003 IEEE, 34th Annual, Vol.4, 15-19 June 2003.

[5] J.Corres, P.Gil, "Instantaneous Speed and Disturbance Torque Observer using Nonlinearity Cancellation of Shaft Encoder", Power Electronics Specialists Conference, PESC'02, 2002 IEEE, 33rd Annual, Vol.2, 23-27 June 2002.

[6] J. Sur, B. Paden, "State observer for linear time-invariant systems with quantized output", Transactions, ASME, Journal of dynamic systems, Measurement and Control. Vol.120, pp. 423-426, 1998

[7] Shunsuke Kobayashi, Abdul Muis, Kouhei Ohnishi, " Sensorless Co-operation

between Human and Mobile Manipulator", IEEE International Conference on Industrial Technology, ICIT 2005, pp 811-816, 14-17 December 2005.

[8]Yu Izumikawa, Kazuhiro Yubai, Junji Hirai; "Fault-Tolerant Control System of Flexible Arm for Sensor Fault by using Reaction Force Observer"; IEEE/ASME Transactions on Mechatronics, Vol. 10, No.4, August 2005

[9] Bing Zheng, Cliff Altemare, and Sohel Anwar; "Fault tolerant Steer-By-Wire road wheel control system"; 2005 American Control Conference

[10]D.U.Campos-Delgado, S.Martinez-Martinez, K.Zhou; "Integrated Fault-Tolerant Scheme for a DC Speed Drive", IEEE/ASME Transactions on Mechatronics, Vol.10, No.4, August 2005

[11] Toshiyuki Murakami, Fangming Yu, Kouhei Ohnishi; "Torque Sensor-less Control in Multi-degree-of–Freedom Manipulator, "IEEE Transactions on Industrial Electronics, Vol.40, No.2, April 1993

[12] Matthew Lawson and Xiang Chen, "Hardware-in-Loop Simulation of Fault Tolerant Control for an Electric Power Steering System", IEEE Vehicle Power and Propulsion Conference, September 2008.

[13] W.S. Levine, The Control handbook, CRC Press; New York: IEEE Press, 1996.

[14] Dan Simon; "Optimal State Estimation"; Wiley-Interscience, 2006

[15] Kemin Zhou with John C. Doyle, Essentials of Robust Control, Prentice Hall, New Jersey, 1998

[16] Xiang Chen and Kemin Zhou, "H_∞ Gaussian Filters on Infinite Time Horizon",

IEEE Transactions on Circuits and Systems-I: Fundamental Theory and Applications, Vol.49, No. 5, May 2002, pp674-679

[17] Guillermo E. Elicabe, Christos Georgakis, "Effect of Feedback Controllers in State Estimation Schemes", American Chemical Society, Ind. Eng. Chem. Res., 2000, *39*, pp387-395, 2000

[18] Xiang Chen, Tiebao Yang, Xiaoqun Chen and Kemin Zhou; " A Generic Model-Based Advanced Control of Electric Power Assisted Steering Systems"; IEEE Transactions on Control Systems Technology, Vol.16, No.6, pp 1289-1300, November 2008

[19] Xiang Chen and Xiaoqun Chen; "Control- Oriented Model for Electric Power Steering System"; Steering and Suspension Technology and Tire and Wheel Technology, SP-2019, 2006 SAE World Congress.

[20] Rajesh Rajamani, Vehicle dynamics and control, New York : Springer, 2005.

[21] Technical Library, MicroMo Electronics, DC Motor Tutorials, DC Motor Application Considerations

http://www.micromo.com/n134479/n.html

[22] Baldor Installation and Operating Manual and Supplement for AC Closed Vector Control Drives, VS1GV

[23] Roboteq Manual for Driver Board AX3500, Rev 2007

[24] Sensor Developments, Operators Manual for Rotating Torque Sensor with Digital Telemetry, Model: 01424

[25] Timothy L. Strunk, Glenn S. Westerman, Patent: 4744041, Method for testing DC motors, International Business Machines Corporation (Armonk, NY) ,1988

[26] P.Baracos, G.Muere, C.A. Rabbath, and W.Jin; "Enabling PC-based HIL Simulation for Automotive Applications", Technical Report, Opal-RT Technologies, Inc.

[27] Ali Tahmesebi, Xiang Chen, "Discrete-Time H_∞ Gaussian Filter", 2006

[28] Yaakov Bar-Shalom, Xiao-Rong Li, Thiagalingam Kirubarajan; "Estimation with applications to tracking and navigation", John Wiley & Sons, Inc., 2001

VITA AUCTORIS

NAME: Smitha Cholakkal

BIRTHDATE: 1984

BIRTHPLACE: Muscat, Sultanate of Oman

EDUCATION:
2007-2009   **Master of Applied Science**
                    Electrical and Computer Engineering
                    University of Windsor, Windsor, ON
                    ⋄ International Graduate Student Scholarship
                    ⋄ Windsor International Graduate Excellence Award

2005-2007   **Master of Engineering,**
                    Mechatronics Engineering
                    Anna University, Chennai, India
                    ⋄ GATE scholarship from Ministry of Human Resources
                      Development, India

2001-2005   **Bachelor in Technology**,
                    Electrical and Electronics Engineering
                    University of Kerala, Kerala, India